



HAL
open science

Weakening Induced by Phase Nucleation in Metamorphic Rocks: Insights From Numerical Models

Marie Baïssset, Philippe Yamato, Thibault Duretz

► **To cite this version:**

Marie Baïssset, Philippe Yamato, Thibault Duretz. Weakening Induced by Phase Nucleation in Metamorphic Rocks: Insights From Numerical Models. *Geochemistry, Geophysics, Geosystems*, 2024, 25 (11), pp.e2024GC011706. 10.1029/2024gc011706 . insu-04780701

HAL Id: insu-04780701

<https://insu.hal.science/insu-04780701v1>

Submitted on 13 Nov 2024

HAL is a multi-disciplinary open access archive for the deposit and dissemination of scientific research documents, whether they are published or not. The documents may come from teaching and research institutions in France or abroad, or from public or private research centers.

L'archive ouverte pluridisciplinaire **HAL**, est destinée au dépôt et à la diffusion de documents scientifiques de niveau recherche, publiés ou non, émanant des établissements d'enseignement et de recherche français ou étrangers, des laboratoires publics ou privés.



Distributed under a Creative Commons Attribution - NonCommercial - NoDerivatives 4.0 International License




Geochemistry, Geophysics, Geosystems®



RESEARCH ARTICLE

10.1029/2024GC011706

Weakening Induced by Phase Nucleation in Metamorphic Rocks: Insights From Numerical Models

M. Baisset¹ , P. Yamato¹ , and T. Duretz² 

¹Univ Rennes, CNRS, UMR 6118, Géosciences Rennes, Rennes, France, ²Institut für Geowissenschaften, Goethe-Universität Frankfurt, Frankfurt, Germany

Key Points:

- Numerical models of work-driven nucleation provide insights on the link between reaction dynamics and weakening in metamorphic rocks
- Weakening follows the nucleation and propagation of plastic shear bands in the vicinity of the reaction products
- Kinetics of heterogeneous nucleation plays a more important role on weakening than physical properties and proportion of reaction products

Supporting Information:

Supporting Information may be found in the online version of this article.

Correspondence to:

M. Baisset,
marie.baisset.pro@gmail.com

Citation:

Baisset, M., Yamato, P., & Duretz, T. (2024). Weakening induced by phase nucleation in metamorphic rocks: Insights from numerical models. *Geochemistry, Geophysics, Geosystems*, 25, e2024GC011706. <https://doi.org/10.1029/2024GC011706>

Received 13 JUN 2024

Accepted 28 OCT 2024

Author Contributions:

Conceptualization: M. Baisset,

P. Yamato

Data curation: M. Baisset

Funding acquisition: P. Yamato

Investigation: M. Baisset

Methodology: M. Baisset, P. Yamato,

T. Duretz

Software: P. Yamato, T. Duretz

Supervision: P. Yamato

Validation: P. Yamato, T. Duretz

Writing – original draft: M. Baisset,

P. Yamato

Abstract Metamorphic transformations involve important changes in material properties that can be responsible for rheological alterations of rocks. Studying the dynamics of these changes is therefore crucial to understand the weakening frequently observed in reactive rocks undergoing deformation. Here, we explore the effects of reaction dynamics on the mechanical behavior of rocks by employing a numerical model where nucleation kinetics and reaction product properties are controlled over time during deformation. Different values are tested for nucleation kinetics, density, viscosity, proportion and size of the reaction products, and pressure-strain rate conditions relative to the brittle-ductile transition. Our results, in good agreement with laboratory and field observations, show that rock weakening is not just a matter of the strength of the reaction products. Both density and viscosity variations caused by the transformation control local stress amplification. A significant densification can by itself generate sufficient stresses to reach the plastic yield of the matrix, even if the nuclei are stronger than their matrix. Plastic shear bands initiate in the vicinity of the newly formed inclusions in response to local stress increases. Coalescence of these shear bands are then responsible for strain weakening. We show that heterogeneous nucleation controlled by mechanical work has an even greater impact than the intrinsic properties of the reaction products. Propagation of plastic shear bands is enhanced between closely spaced nuclei that generate significant stress increases in their vicinity. This study highlights the importance of transformational weakening in strong rocks affected by fast reaction kinetics close to their brittle-ductile transition.

Plain Language Summary When rocks are subjected to changes in pressure and temperature, for example, in areas of the Earth where tectonic plates collide, their constitutive minerals are no longer stable and react to form new phases of different physical properties. These changes can trigger significant stress reductions, a process known as weakening, which involves a concentration of the strain in specific areas sometimes associated with earthquakes. In order to better understand and quantify the effects of reaction dynamics on the way rocks deform, we use specialized computer code in which we can vary the reaction and strain rates, as well as the physical properties of the deformed material and its reaction products. Our results are in good agreement with results from deformation experiments in the laboratory and field observations on natural rocks. They show that nucleation of dense reaction products, a common case for high pressure transformations, is responsible for a local stress increase in the vicinity of the nuclei. This increase triggers fracture initiation and associated weakening. When nucleation is enhanced by the energy produced in highly strained areas, reaction products nucleate in close proximity to each other, which highly contributes to local stress increases and to the process of embrittlement.

1. Introduction

Metamorphic transformations on Earth are known to affect rocks that experience a change in P - T conditions. Phase transformations concomitant with deformation have been proposed to explain the strain localization frequently observed in natural rocks (Austrheim & Boundy, 1994; Boundy et al., 1992; Brodie & Rutter, 1985; Furusho & Kanagawa, 1999; Handy & Stünitz, 2002; Hidas et al., 2013; John et al., 2009; Keller et al., 2004; Lund & Austrheim, 2003; Lund et al., 2004; Newman et al., 1999, 2021; Précigout et al., 2007; Rogowitz & Huet, 2021; Rubie, 1983; Scambelluri et al., 2017). Such localization consists of viscous shear zones or brittle fractures. Transformational weakening associated with strain localization has also been investigated in the laboratory on monomineralic and polymineralic aggregates of rock forming minerals deformed out of their stability field (Baisset et al., 2024; De Ronde et al., 2005; Incel et al., 2019, 2020; Mansard et al., 2020; Marti et al., 2018; Shi

© 2024 The Author(s). Geochemistry, Geophysics, Geosystems published by Wiley Periodicals LLC on behalf of American Geophysical Union. This is an open access article under the terms of the [Creative Commons Attribution-NonCommercial-NoDerivs License](https://creativecommons.org/licenses/by/4.0/), which permits use and distribution in any medium, provided the original work is properly cited, the use is non-commercial and no modifications or adaptations are made.

Writing – review & editing: M. Baïssset, P. Yamato, T. Duretz

et al., 2018; Stünitz & Tullis, 2001; Zheng et al., 2019). Several mechanisms have been proposed to explain such weakening (Bras et al., 2021; De Ronde et al., 2005; Holyoke & Tullis, 2006b; Stünitz & Tullis, 2001; Yamato et al., 2022):

1. Nucleation of weak phases (Gueydan et al., 2003; Mitra, 1978; Oliot et al., 2010; Rubie, 1990; White & Knipe, 1978). Strength contrasts induced by the transformation generate stress concentrations around the weak isolated phases that locally begin to connect either by plastic deformation or by brittle failure (Holyoke & Tullis, 2006c). This process can eventually lead to stress transfer into the stronger matrix (Ferrand et al., 2017).
2. Nucleation of fine-grained and mixed phases, unfavorable for growth, that cause a switch from grain size insensitive deformation mechanisms to grain boundary controlled processes such as diffusion accommodated grain boundary sliding (Boullier & Gueguen, 1975; Brodie & Rutter, 2000; Burnley & Green, 1989; Gerald & Stünitz, 1993; Giuntoli et al., 2018; Handy, 1989; Hidas et al., 2013; Holyoke & Tullis, 2006a; Kenkmann & Dresen, 2002; Kerrich et al., 1980; Klaper, 1990; Newman et al., 1999; Rubie, 1983, 1990; Rutter & Brodie, 1988a, 1988b; Snow & Yund, 1987; Stünitz & Gerald, 1993; Stünitz & Tullis, 2001; Stünitz et al., 2020; Wenk & Pannetier, 1990). This process can eventually lead to faulting if the ratio between the strain rate and the reaction rate is satisfactory for fast sliding on the reaction products, with possible activation of thermal runaway mechanisms (Incel et al., 2017, 2019; John et al., 2009; Shi et al., 2018, 2022; Thielmann, 2018; Thielmann et al., 2015).
3. Faulting caused by pore pressure increase (Alvizuri & Hetényi, 2019; Brantut et al., 2012; Dobson et al., 2002; Gasc et al., 2022; Hacker et al., 2003; Hetényi et al., 2007; Jung et al., 2004; Murrell & Ismail, 1976; Okazaki & Hirth, 2016; Olgaard et al., 1995; Omori et al., 2004; Paterson, 1989; Raleigh & Paterson, 1965; Rutter & Brodie, 1988a) or hydrolytic weakening (Chen et al., 2006; De Ronde et al., 2004; Holyoke & Tullis, 2006a; Kohlstedt, 2006; Kronenberg et al., 1990; Schmidt et al., 2003; Stünitz & Tullis, 2001; Tullis & Yund, 1980) in the case of dehydration reactions.
4. Volume change induced by the transformation, a process mostly described in the case of polymorphic transformations and called “transformation plasticity” or “transformational superplasticity” (Burnley et al., 1991; Dunand et al., 2001; Incel et al., 2019; Johnson et al., 2021; Kelemen & Hirth, 2012; Kirby et al., 1996; Malvoisin et al., 2017, 2020, 2021; Meike, 1993; Poirier, 1982; Schmalholz et al., 2020; Schmidt et al., 2003; Ulven et al., 2014; Yamato et al., 2022).

Previous studies have focussed on the mechanical behavior of polyphase rocks based on deformation experiments (e.g., Dimanov & Dresen, 2005; Ji et al., 2001; Jin et al., 2001; Rogowitz et al., 2023; Xiao et al., 2002) as well as numerical studies (e.g., Beall et al., 2019; Cyprych et al., 2016; Dabrowski et al., 2012; Jessell et al., 2009; Rogowitz et al., 2023; Yamato et al., 2019, and references therein). They showed that a strength contrast between the phases is of major importance for strain localization, and that the switch in deformation mode of the whole rock (i.e., from ductile to brittle) is much more complex than in single phase materials. For example, the brittle-ductile transition of a polyphase rock can not be represented by a line in the P - T space as for homogeneous materials, but rather by a “semi-brittle” field where boundaries are not clearly defined. Indeed, deformation modes can be different for each phase at a given condition (Beall et al., 2019; Marti et al., 2017; Rogowitz et al., 2023; Yamato et al., 2019). Phase interactions can even cause brittle behavior in phases that would have been ductile if deformed as single phases. However, the majority of these studies only consider a constant rock mineralogy, with fixed proportions of weak and strong phases that do not vary from the beginning to the end of the experiments (or simulations). Metamorphism is nevertheless a dynamic process that involves a change in phase proportions with time, following a defined reaction rate (i.e., kinetics).

Some studies have instead focused on the theory, quantification and modeling of reaction products nucleation and growth in reactive geological materials (Gaidies, 2017; Gaidies et al., 2011; Ketcham & Carlson, 2012). However, the parameters governing these processes remain unknown for the majority of important geological transformations (e.g., eclogitization of mafic and felsic rocks at depth). Nucleation kinetics are particularly poorly constrained, although they appear fundamental to understand the mechanical instabilities known to be triggered by the very first stages of the transformation (Baïssset et al., 2024; Incel et al., 2019; Wayte et al., 1989). In addition, if the conditions required to trigger the transformation at the expected P - T conditions are not met (e.g., absence or lack of free H_2O/OH^-), rocks can be brought out of their stability field without transforming. This metastable state can strongly enhance local kinetics in places where the energy required to trigger the transformation is reached (Wayte et al., 1989), a notion expressed in the nucleation and growth equations through the Gibbs free energy term (Rubie, 1998). Eventually, metamorphic transformations are usually concomitant with

deformation, which has not been modeled in previous numerical studies focusing on mineral nucleation and growth.

As these aspects which are crucial for understanding the mutual interactions between deformation and synchronous transformations remain under-explored, we here conduct a series of numerical models where an initially homogeneous matrix is deformed while undergoing transformation. The aim of this study is to test the effect on the mechanical behavior of the system of the nucleation of inclusions which properties differ from those of the initial material. For that purpose, we designed a two-dimensional numerical model in which inclusions of varying strength and density nucleate according to a defined reaction rate, during the deformation of a viscous matrix.

2. Methods

2.1. Modeling Strategy

In this study, we particularly focus on the behavior of rocks undergoing transformation at high P - T conditions, as in subduction environments for example. We chose this particular context to tackle the issue of rock embrittlement below the classical seismogenic zone. Indeed, a growing number of studies suggest that metamorphic transformations could be responsible for failure at depth in areas where rocks are expected to be ductile (Austrheim & Boundy, 1994; Hacker et al., 2003; Hetényi et al., 2007; Jung et al., 2004; Nakajima et al., 2013). As we want to discuss the evolution of stresses while the material is reacting, we performed our simulations at laboratory strain rates ($\dot{\epsilon}_{BG} = 10^{-5} \text{ s}^{-1}$). This allows us to directly compare our results to those of experimental work, and to study the dynamics of the mechanisms involved.

To carry out this study, we proceed in two stages. First, we define a reference model where random nucleation takes place in the matrix with the reaction products being weaker, but not denser than the initial material (Table 1). We study the effect of local viscosity and density variations induced by nucleation, by running simulations where the magnitude of these variations are systematically varied. Results of these simulations are then compared to that of the reference model (Table 1). In a second step, we define a model which parameters have been chosen to generate a maximum weakening (Wd_WD, Table 1), including three of the four weakening mechanisms mentioned in Section 1: the nucleation of weak (item 1) and fine-grained phases (item 2) that change in density compared to their matrix (item 4). Weakening induced by dehydration reactions (item 3) is not considered here as fluid flow is not implemented in our numerical code. Reaction products in this second model are weaker than the matrix to model the nucleation of either weaker phases or very fine-grained assemblages in the absence of grain growth. Reaction products in this model are also denser than the matrix which is consistent with the case of a metamorphic transformation that takes place at high pressure during burial of the rocks. In addition, the nuclei are not purely randomly distributed in the matrix, but are preferentially placed in areas of the model where the mechanical work is the highest. This represents enhanced nucleation in highly strained zones, for example due to increased surface area for nucleation in these domains of high internal strain energy (e.g., crystalline defects: dislocations, twins and cracks, or grain boundaries; Cahn, 1957; Holyoke & Tullis, 2006b; Incel et al., 2023; Rubie, 1998; Rubie & Thompson, 1985). This process of heterogeneous nucleation is responsible for strain localization in reactive rocks as observed in experimental samples (De Ronde et al., 2004; Holyoke & Tullis, 2006a; Stünitz & Tullis, 2001) and natural rocks (Brodie & Rutter, 1985; Wayte et al., 1989). Evolution of the Wd_WD model is then used as a comparison against models of varying parameters: size of the reaction products, nucleation kinetics, fixed proportions of weak inclusions, and P - $\dot{\epsilon}$ conditions relative to the brittle-ductile transition. All performed simulations and their parameters are summarized in Table 1.

In the following, we will first describe the way these two models are designed, specify the value of the parameters chosen, and present the numerical code used. In a second step, validation tests are presented, followed by the results of the parametric studies for the two sets of models. Results and limitations of our work will then be discussed in the light of previous studies on the topic.

2.2. Model Setup

The initial model consists of an anorthite matrix of $1 \text{ mm} \times 0.5 \text{ mm}$, which could be seen as an enlargement inside a deformation jacket such as the ones used in experimental studies (usually cylinders of $10 \times 5 \text{ mm}$ in Griggs-type apparatuses). A strain rate of $\dot{\epsilon}_{BG} = 10^{-5} \text{ s}^{-1}$ is applied on the box which is deformed under pure-shear (Figure 1a). At this high strain rate, high temperatures are required for the matrix to be ductile. Consequently,

Table 1
Summary of the Simulations Performed in This Study

Name/nucleation style	Kinetics	η_m/η_n^a	$\Delta\rho$ (kg.m ⁻³)	Size ^b (μ m)	P (GPa)	$\dot{\epsilon}$ (s ⁻¹)	n^c	Figures ^d
Models with fixed proportions of nuclei								
Homogeneous ($X = 0\%$)	–	–	–	–	2.0	10 ⁻⁵	1	Figures 2 and 3
X_5 ($X = 5\%$)	–	>1	+400	10	2.0	10 ⁻⁵	1	Figure 8 and Figure S10 in Supporting Information S1
X_{10} ($X = 10\%$)	–	>1	+400	10	2.0	10 ⁻⁵	1	Figure 8 and Figure S10 in Supporting Information S1
X_{20} ($X = 20\%$)	–	>1	+400	10	2.0	10 ⁻⁵	1	Figure 8 and Figure S10 in Supporting Information S1
Models with random nucleation								
Reference (Weak $\Delta\rho\{0\}$)	k_2	>1	0	10	2.0	10 ⁻⁵	1	Figures 2–6; Figures S3 and S4 in Supporting Information S1
Weak $\Delta\rho\{-400\}$	k_2	>1	-400	10	2.0	10 ⁻⁵	1	Figure 3
Weak $\Delta\rho\{+200\}$	k_2	>1	+200	10	2.0	10 ⁻⁵	1	Figure 3
Weak $\Delta\rho\{+400\}$	k_2	>1	+400	10	2.0	10 ⁻⁵	1	Figures 3 and 6; Figures S4 and S8 in Supporting Information S1
Weak $\Delta\rho\{+400\}$ salt	k_2	>1	+400	10	2.0	10 ⁻⁵	1	Figure 9
$\Delta\rho\{+400\}$	k_2	1	+400	10	2.0	10 ⁻⁵	1	Figure 3 and Figure S4 in Supporting Information S1
Strong $\Delta\rho\{0\}$	k_2	<1	0	10	2.0	10 ⁻⁵	1	Figure 3 and Figure S5 in Supporting Information S1
Strong $\Delta\rho\{-400\}$	k_2	<1	-400	10	2.0	10 ⁻⁵	1	Figure 3 and Figure S5 in Supporting Information S1
Strong $\Delta\rho\{+400\}$	k_2	<1	+400	10	2.0	10 ⁻⁵	1	Figure 3 and Figure S5 in Supporting Information S1
Models with work-driven nucleation (Wd)								
Wd_W (Weak)	k_2	>1	0	10	2.0	10 ⁻⁵	1	Figures 4 and 6; Figure S8 in Supporting Information S1
Wd_WD (Weak & Dense)	k_2	>1	+400	10	2.0	10 ⁻⁵	1	Figures 4–9; Figures S5–S12 in Supporting Information S1
Wd_WD_ k_1	k_1	>1	+400	10	2.0	10 ⁻⁵	1	Figure 7
Wd_WD_ X_5^c	k_2	>1	+400	10	2.0	10 ⁻⁵	1	Figure 8
Wd_WD_salt	k_2	>1	+400	10	2.0	10 ⁻⁵	1	Figure 9
Wd_WD_5 μ m	k_2	>1	+400	5	2.0	10 ⁻⁵	1	Figure S9 in Supporting Information S1
Wd_WD_20 μ m	k_2	>1	+400	20	2.0	10 ⁻⁵	1	Figure S9 in Supporting Information S1
Wd_WD_2.5 GPa	k_2	>1	+400	10	2.5	10 ⁻⁵	1	Figure S11 in Supporting Information S1
Wd_WD_slow	k_2	>1	+400	10	2.0	10 ^{-5.5}	1	Figure S11 in Supporting Information S1
Wd_WD_n ₃	k_2	>1	+400	10	2.0	10 ⁻⁵	3	Figure S12 in Supporting Information S1

^aViscosity ratio between matrix and nuclei. ^bDiameter of the nuclei. ^cStress exponent. ^dMain figures where model results are shown. ^eReaction stopped at $X = 5\%$. All models were run at 800°C.

simulations have been performed at 800°C. The background pressure is set to 2 GPa. These values lie in the range of achievable laboratory conditions on plagioclase-bearing rocks. In that way, our models can be regarded as deformation simulations of a plagioclase matrix undergoing eclogitization at high pressure and laboratory strain rates (Baïssset et al., 2024; Incel et al., 2019; Shi et al., 2018; Stünitz & Tullis, 2001). In addition, the P - T - $\dot{\epsilon}$ conditions chosen lie above the breakdown reaction of anorthite into zoisite, kyanite and quartz, but below the transformation of albite into jadeite (Figure 1c). Running simulations at such conditions is therefore of particular interest if we want to avoid the problem of considering two different transformations that are known to have different kinetics and different mechanical consequences (Baïssset et al., 2023).

The model is initially composed of a homogeneous matrix of anorthite with a constant viscosity of $5 \cdot 10^{13}$ Pa·s. This constant value corresponds to the viscosity that can be calculated at the conditions of the simulations for wet anorthite under dislocation creep (Rybacki & Dresen, 2000). Weak reaction products nucleate in the matrix with time in the form of circular inclusions with 10 μ m diameter. The nuclei are four orders of magnitude weaker than the matrix ($5 \cdot 10^9$ Pa·s). This value corresponds to the viscosity that can be calculated at the conditions of the simulations for 0.1 μ m grains of wet anorthite under diffusion creep (Rybacki & Dresen, 2000). Inclusions that

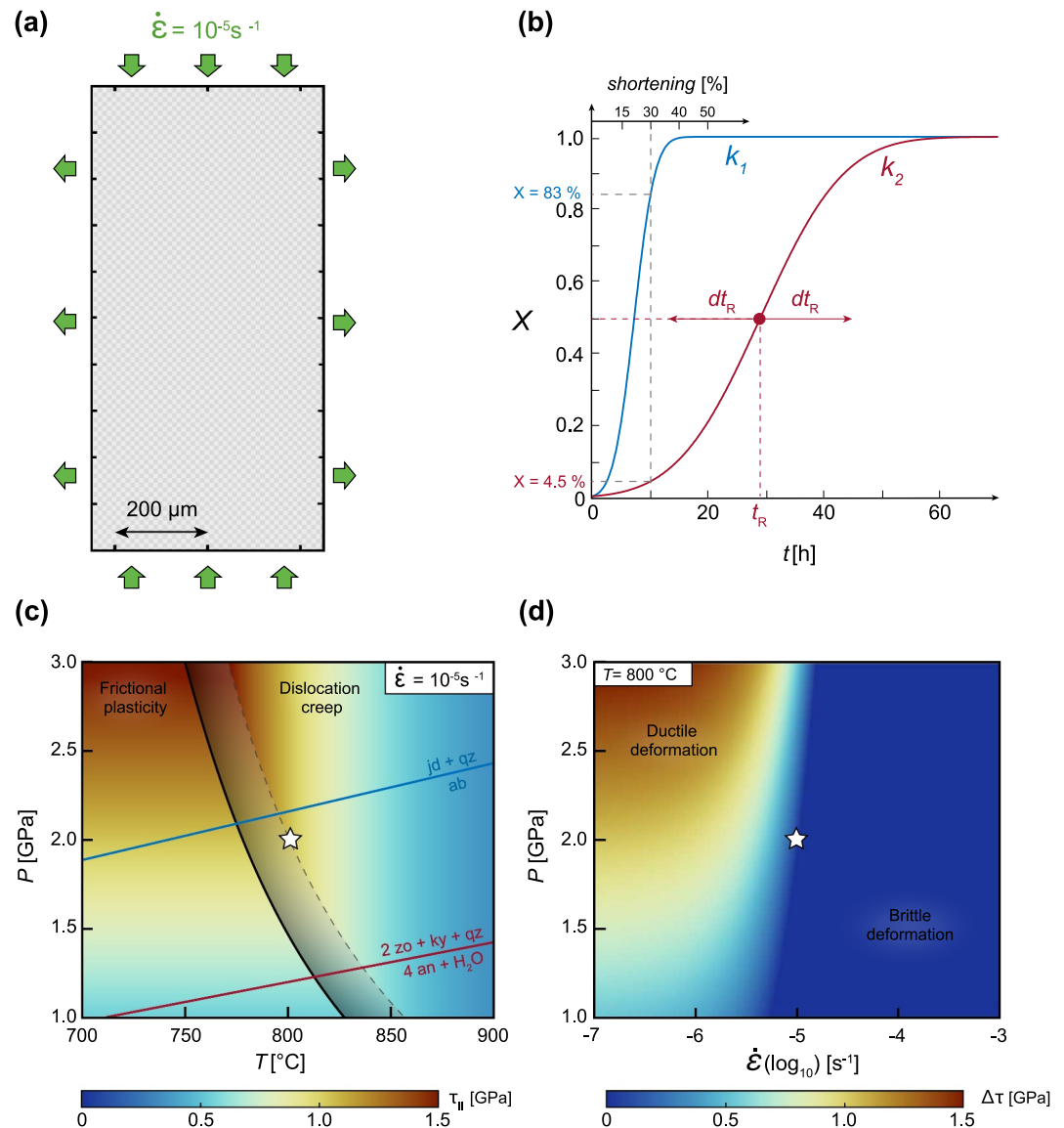


Figure 1. (a) Model setup. The gray checkerboard is used for visualization of matrix deformation and represents a material of homogeneous properties. (b) Kinetic laws (k_1 and k_2) used in our models. X corresponds to the amount of reaction products and depends on two parameters: t_R and dt_R (see text for details). For kinetics k_1 , $t_R = 7.3$ hr and $dt_R = 4.0$ hr and for kinetics k_2 , $t_R = 29.1$ hr and $dt_R = 16.0$ hr. Shortening of the box is also represented along the time axis. At 30% shortening, reaction extent reaches 83% in models with kinetics k_1 while it reaches 4.5% in models with kinetics k_2 . (c) Second invariant of the stress tensor in the P - T space for wet anorthite (Rybacki & Dresen, 2000, with creep parameters $n = 3.0$, $A = 3.9811 \cdot 10^{-16} \text{ Pa}^{-n} \cdot \text{s}^{-1}$, $Q = 356 \text{ kJ} \cdot \text{mol}^{-1}$) at a strain rate of $\dot{\epsilon} = 10^{-5} \text{ s}^{-1}$. The dotted black line indicates the domain where frictional behavior is possible (on the left of the line). The area located on the left of the bold black line corresponds to the domain where frictional plasticity is the dominant deformation mechanism. Plagioclase breakdown reactions are indicated. jd: jadeite, qz: quartz, ab: albite, zo: zoisite, ky: kyanite, an: anorthite. (d) Values of $\Delta\tau$, the difference between the yield stress and the shear stress supported by the matrix (calculated as in Yamato et al. (2022)), in the P versus $\dot{\epsilon}$ diagram for the chosen linear viscosity of the matrix ($5 \cdot 10^{13} \text{ Pa}\cdot\text{s}$) at $T = 800^\circ\text{C}$.

appear in the matrix during the simulation therefore represent reactive zones where very fine-grained phases nucleate. In some of the models, the density of the reaction products is different from the density of the matrix. Because the total volume of the box is conserved during the simulation, these local density variations imply that mass balance is not conserved. Models with reaction products denser than their matrix can therefore be regarded as (a) open systems where gains and losses of the elements required for the transformation are allowed, or (b)

Table 2
Parameters Used in This Study

Parameters	Symbol	Units	Matrix	Reaction products	References
Viscous properties					
Constant linear viscosity	η	Pa · s	$5 \cdot 10^{13}$	$5 \cdot 10^9$ (weak) $5 \cdot 10^{17}$ (strong)	
Elastic properties					
Shear modulus	G	Pa	$4.0 \cdot 10^{10}$	$4.0 \cdot 10^{10}$	Pabst et al. (2015)
Drucker-Prager plasticity					
Cohesion	C	Pa	$50 \cdot 10^6$	$50 \cdot 10^6$	
Friction	φ	°	30	30	
Viscosity of regularization	η^{VP}	Pa · s	10^{11}	10^{11}	
Other properties					
Density	ρ	kg · m ⁻³	2,850	3,250 (for Wd_WD models)	

materials where the nucleation of very fine-grained clusters leads to local porosity reduction (i.e., compaction). In our models, the phases can deform in three ways: elastically (Hooke's law), viscously, and frictionally following a Drucker-Prager law (see Section 2.4). Considering frictional rheology is particularly important when the material is deformed at conditions close to the yield stress (Figures 1c and 1d), a choice that will be discussed later. Material properties used for the matrix and reaction products are presented in Table 2.

2.3. Choice of Nucleation Kinetics

In solid state transformations, kinetics (i.e., reaction rate) of the transformation from one phase to another is described by the Johnson-Mehl-Avrami-Kolmogorov equation (Avrami, 1939):

$$X = 1 - \exp(-Kt^n) \quad (1)$$

where X corresponds to the reaction extent at time t . K and n are constants that depend on the style of nucleation and growth of the considered reaction. For reactions with $n > 1$, the reaction progress follows an S-shape trend (as in Figure 1b). The initial slope of this S-shape curve is attributed to the nucleation phase, while the following steep slope constitutes the growth-controlled part of the transformation. Eventually, the reaction rate decreases again, as few material remains available for further nucleation. As the values of K and n are poorly constrained for the type of metamorphic reaction modeled here, we merely compute reaction kinetics as an S-shape law using a cumulative distribution function for a normal distribution (Figure 1b). For the sake of simplicity, we consider a system in which nucleation is the dominant controlling mechanism, and growth of the reaction products is not considered. However, the computed S-shape law well describes the studied system, as we only focus on the first increments of transformation (i.e., the nucleation-dominated part of the S-shape curve). Indeed, previous studies already emphasized that a very small amount of reaction products can have strong mechanical consequences, and reaction-induced softening is often associated with nucleation-controlled transformations rather than growth-controlled transformations (Baïssset et al., 2024; Incel et al., 2019; Mansard et al., 2020; Rubie, 1983; Shi et al., 2018). Moreover, pure-shear experiments are only performed over hours to a few days, which do not allow large reaction extent. The equation of an S-shape curve (Equation 2) depends on two parameters:

$$X = 1 - 0.5 \cdot \operatorname{erfc}\left(-\frac{(t_R - t)}{dt_R}\right) \quad (2)$$

where X goes between 0 (not reacted) and 1 (fully reacted), t is the time, t_R is the time required for reaching a quantity of $X = 50\%$ reaction products and dt_R represents the slope of the curve: $dt_R = \sigma/\sqrt{2}$ where σ is the standard deviation. For the reference model, t_R is set to 29.1 hr and dt_R to 16.0 hr (kinetics k_2 ; Figure 1b). These

values have been chosen to generate a small reaction extent during the 10–20 hr of the simulation (corresponding to 30%–50% shortening), as usually observed in laboratory experiments.

2.4. Mathematical Formulation

Numerical models were designed using the same 2D thermo-mechanical compressible code as in Yamato et al. (2022) and Luisier et al. (2023) (MDoodz). This code solves the continuity and momentum equations (with the effect of gravity and inertia neglected):

$$\frac{d\ln(\rho)}{dt} = -\frac{\partial v_i}{\partial x_i} \quad (3)$$

$$\frac{\partial \sigma_{ij}}{\partial x_j} = 0 \quad (4)$$

where ρ is the density, σ_{ij} the stresses, and i represents the coordinate index for the velocity (v_i) and spatial coordinate (x_i). The thermal evolution of the models is described by:

$$\rho C_p \frac{DT}{Dt} = \frac{\partial}{\partial x_i} \left(k \frac{\partial T}{\partial x_i} \right) + H_s \quad (5)$$

where C_p is the heat capacity, T is the temperature, and k is the thermal conductivity. Shear heating H_s is defined as:

$$H_s = \tau_{ij} \left(\dot{\epsilon}_{ij} - \dot{\epsilon}_{ij}^e \right) \quad (6)$$

where $\dot{\epsilon}_{ij}$ is the deviatoric strain rate tensor and $\dot{\epsilon}_{ij}^e$ its elastic part.

Equations 3–6 are discretized over a rectangular model domain using staggered grid finite differences. The spatial discretization of material properties on the grid (rheological and thermal parameters) is provided via Lagrangian markers (Gerya & Yuen, 2003). At each time step, material and thermal properties defined on the markers are interpolated to the nodes in the finite difference mesh using a distance-dependent interpolation (1-cell interpolation; see Yamato et al., 2012). All marker positions are evolved forward in time using a fourth order (in space) Runge-Kutta scheme (with a Courant number set to 0.2).

In this study, we use a visco-elasto-frictional rheological model. The contribution of each deformation mechanism is computed iteratively in order to satisfy the following Maxwell model (see Yamato et al., 2022):

$$\dot{\epsilon}_{ij} = \dot{\epsilon}_{ij}^v + \dot{\epsilon}_{ij}^e + \dot{\epsilon}_{ij}^{vp} \quad (7)$$

where v, e and vp superscripts refer to the viscous, elastic, and viscoplastic amounts of strain rate (V-E-VP formulation, Duretz et al., 2021). We used constant linear viscosities, so that the flow stress (τ_v) is expressed as:

$$\tau_v = 2\eta \dot{\epsilon}_{II} \quad (8)$$

where $\dot{\epsilon}_{II}$ is the square root of the second invariant of the strain rate tensor. Consequently, the viscous strain rate ($\dot{\epsilon}_{ij}^v$) is computed as:

$$\dot{\epsilon}_{ij}^v = \frac{\tau_{ij}}{2\eta} \quad (9)$$

The yield stress (τ_y) is expressed as:

$$\tau_y = C \cos(\varphi) + P \sin(\varphi) + \eta^{vp} \dot{\epsilon}_{II}^{vp} \quad (10)$$

and depends on the pressure P (that corresponds to the negative of mean stress), C and φ , the cohesion and the friction angle of the material, respectively (see Table 2). η^{VP} is the viscosity of regularization and $\dot{\epsilon}_{\text{II}}^{\text{VP}}$ is the square root of the second invariant of the viscoplastic strain rate tensor (Duretz et al., 2020). Consequent strain rate for viscoplasticity (frictional behavior) is computed by:

$$\dot{\epsilon}_{ij}^{\text{VP}} = \dot{\epsilon}_{\text{II}}^{\text{VP}} \frac{\tau_{ij}}{\tau_{\text{II}}} = \left[\dot{\epsilon}_{\text{II}} - \frac{\dot{\tau}_{ij}}{2G} - \frac{\tau_{\text{II}}}{2\eta} \right] \frac{\tau_{ij}}{\tau_{\text{II}}} \quad (11)$$

where G is the shear modulus (see Table 2). This contribution of viscoplasticity is only computed when the yield criterion is met. The effective viscosity (η), which relates the deviatoric stress tensor and the strain rate tensor, is computed once Equation 7 is satisfied and takes the form of:

$$\eta = \frac{\tau_{ij}}{2\dot{\epsilon}_{ij}} = \frac{\tau_{\text{II}}}{2\dot{\epsilon}_{\text{II}}} \quad (12)$$

Finally, the elastic strain rate is expressed following Hooke's law as:

$$\dot{\epsilon}_{ij}^{\text{e}} = \frac{\dot{\tau}_{ij}}{2G} \frac{\tau_{ij}}{\tau_{\text{II}}} \quad (13)$$

by computing the Jaumann derivative of the deviatoric stress tensor (Jaumann, 1911; Moresi et al., 2021). In the 2D Cartesian case, where i and j correspond to the x and y direction, the second invariant of the deviatoric stress tensor can be computed as:

$$\tau_{\text{II}} = \sqrt{\frac{1}{2}(\tau_{xx}^2 + \tau_{yy}^2) + \tau_{xy}^2} \quad (14)$$

and the total work rate which is defined as:

$$\dot{W}_{\text{tot}} = \tau_{ij} \dot{\epsilon}_{ij} \quad (15)$$

can also be written as:

$$\dot{W}_{\text{tot}} = \tau_{xx} \dot{\epsilon}_{xx} + \tau_{yy} \dot{\epsilon}_{yy} + \tau_{xy} \dot{\epsilon}_{xy} + \tau_{yx} \dot{\epsilon}_{yx} \quad (16)$$

Replacing strain rates $\dot{\epsilon}_{ij}$ in Equation 15 by:

$$\dot{\epsilon}_{ij} = \frac{\tau_{ij}}{2\eta} \quad (17)$$

We obtain in the 2D Cartesian case:

$$\dot{W}_{\text{tot}} = \frac{1}{2\eta} (\tau_{xx}^2 + \tau_{yy}^2 + \tau_{xy}^2 + \tau_{yx}^2) \quad (18)$$

or using the condition of force balance $\tau_{ij} = \tau_{ji}$:

$$\dot{W}_{\text{tot}} = \frac{1}{2\eta} (\tau_{xx}^2 + \tau_{yy}^2 + 2\tau_{xy}^2) = \frac{1}{\eta} \left[\frac{1}{2} (\tau_{xx}^2 + \tau_{yy}^2) + \tau_{xy}^2 \right] \quad (19)$$

which is equal to:

$$\dot{W}_{\text{tot}} = \frac{\tau_{\text{II}}^2}{2\eta} \quad (20)$$

Hence, the total work at each time step can be expressed as:

$$W_{\text{tot}} = \dot{W}_{\text{tot}} dt \quad (21)$$

2.5. Location of the Nuclei at Each Time Step

While in the reference model reaction products are randomly placed in the matrix over time, nuclei in the weakest reference model are preferentially placed in areas where the mechanical work is high. The procedure used to determine the position of the nuclei is very similar to that of Ketcham and Carlson (2012). At each time step, to choose the location of a newly formed inclusion, we first integrate over time the total work rate on each cell of the model (i.e., the sum of elastic work and dissipative work; Figures S1c and S2c in Supporting Information S1; Equation 20). This integrated work is then normalized to the total work of the model and interpolated on the markers. Values of this normalized integrated work are sorted following a cumulative density function in which a value between 0.5 and 1 is randomly picked. The chosen value then determines the marker which will host the center of the new inclusion. All markers that lies in the area of the inclusion, defined by its center and a diameter of 10 μm , are then checked to avoid placing the new nucleus on an already existing one. If necessary, the procedure is repeated until a suitable position is found for the inclusion.

3. Results

3.1. Model Validation and Resolution Tests

For model validation, a first simulation was run with a homogeneous matrix of anorthite where nucleation has been switched-off (homogeneous, Table 1 with parameters summarized in Table 2). Results from this simulation were compared with results from the analytical solution for shear stress evolution, and semi-analytical solutions for strain rate and work rate repartition, following equations of Section 2.4. Results for visco-elastic and visco-elasto-viscoplastic formulations are shown in Figures S1 and S2 in Supporting Information S1, respectively. Verification of our numerical models is confirmed by the very good match between our two-dimensional simulations and the analytical solutions.

Results of the resolution tests are shown in Figure S3 in Supporting Information S1. The difference between the highest resolution model (1600 \times 1600 cells) and lower resolution models was computed for the effective stress using a measure of the discretization error (Error_{1600} ; Figure S3b in Supporting Information S1). Error_{1600} decreases with decreasing grid spacing (dx ; Figure S3b in Supporting Information S1), with a slope of about -1 in the $\log_{10}(\text{Error}_{1600})$ versus $\log_{10}(1/dx)$ plot, which means that the discretization error decreases by a factor 2 when the grid spacing is divided by 2. As the resolution increases, the evolution of the effective stress is getting closer to that of the 1600 \times 1600 model (Figure S3a in Supporting Information S1). The same information can be visually assessed for the accumulated strain pattern (Figures S3c–S3f in Supporting Information S1). Good convergence of the results therefore leads us to run models of 800 \times 800 cells in the rest of the study.

3.2. Evolution of the Reference Model

Effective stress evolution of the reference model (Table 1) compared to the homogeneous model is represented on Figure 2b. We can see that the reference model undergoes a pronounced weakening with strength decreasing from ~ 950 MPa at 5% shortening to ~ 570 MPa at 40% shortening when the reaction extent is close to 9% (Figure 2a). Evolution of the accumulated plastic strain (Figure 2c) shows that deformation of the model is controlled by brittle deformation of the matrix, with fractures initiating in the vicinity of weak nuclei (Figure S4a in Supporting Information S1) before coalescing through time.

3.3. Effect of Reaction Product Strength

To assess the effect of the strength of the reaction products, we designed a model in which the nuclei are stronger than the matrix ($\text{Strong}\Delta\rho\{0\}$, Table 1), that is, which nuclei have a viscosity four orders of magnitude higher than their matrix (Table 2). Results from this model indicate that nucleation of stronger reaction products does not

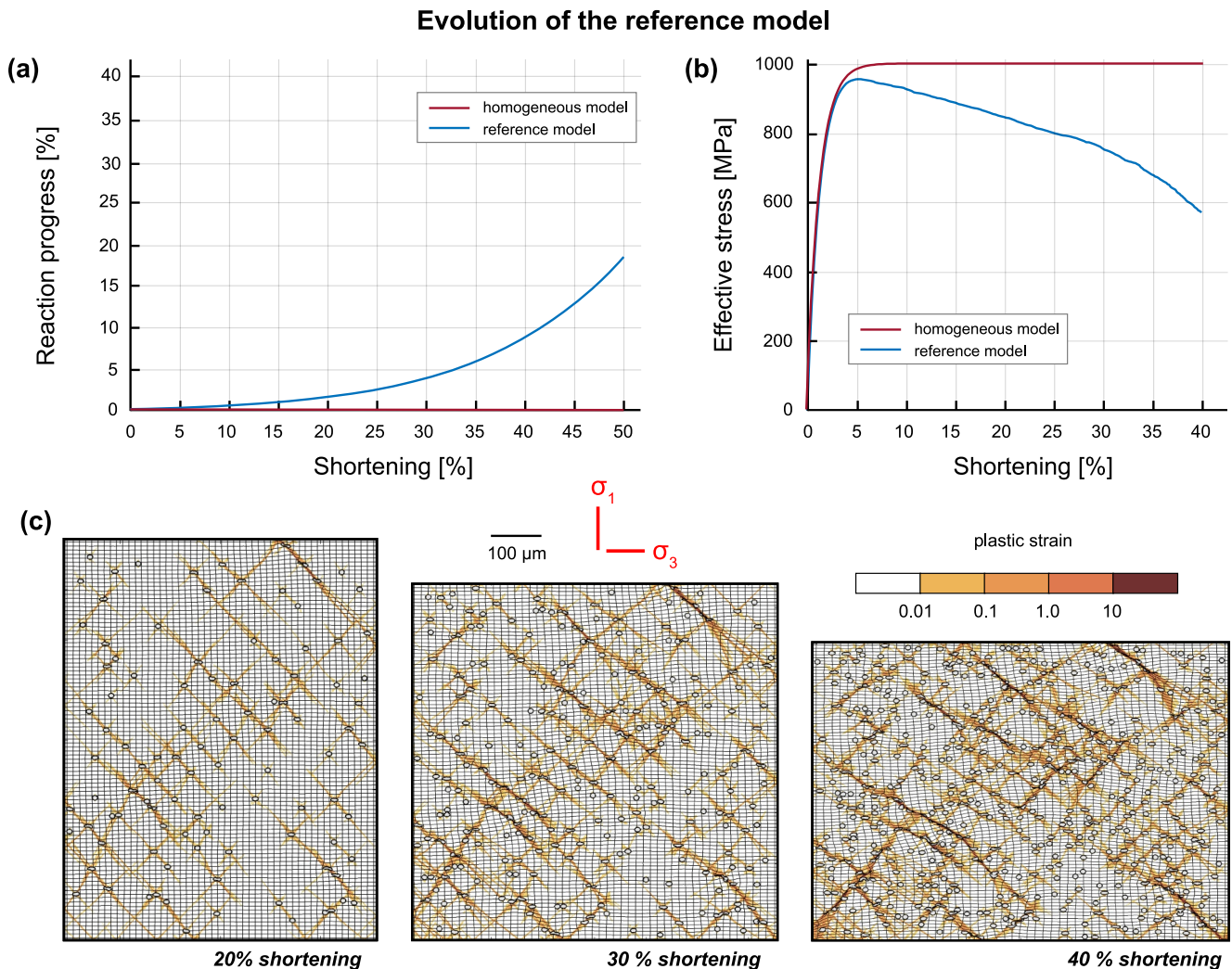


Figure 2. Evolution of the reference model (see Table 1 for details). Reaction progress (a) and effective stress (b) are represented as a function of the amount of shortening and compared to the evolution of the homogeneous model. (c) From left to right: accumulated plastic strain of the reference model at 20%, 30%, and 40% shortening.

affect the mechanical behavior of the material (i.e., effective stress evolution is similar to the stress evolution of the homogeneous model; Figure 3a).

3.4. Density Variations

Simulations with different amplitudes of the density difference between the nucleating inclusions and their matrix were performed to study the effect of density variations on the mechanical evolution of the material (Weak $\Delta\rho$ {-400}, Weak $\Delta\rho$ {+200}, Weak $\Delta\rho$ {+400}, Strong $\Delta\rho$ {-400}, $\Delta\rho$ {+400} and Strong $\Delta\rho$ {+400}, Table 1; Figures 3b–3d). Results of these simulations show that a densification of 400 kg.m⁻³ induces a significant weakening of the material (Figure 3b).

This weakening is pronounced for the model with nuclei stronger than their matrix (Strong $\Delta\rho$ {+400}). It is also pronounced for the model with nuclei of the same viscosity than their matrix ($\Delta\rho$ {+400}). Both models present a strength reduction of 450 MPa at 40% shortening due to densification. For the model with weak nuclei (Weak $\Delta\rho$ {+400}), the strength reduction due to densification only is lower (211 MPa at 40% shortening) but it nevertheless adds to the weakening caused by a low viscosity of the nuclei. In our models, densification is responsible for a decrease of the mean pressure (e.g., Figure S5c in Supporting Information S1) in addition to a local stress increase around the nuclei (Figure S4b in Supporting Information S1). The yield stress of the material can therefore easily

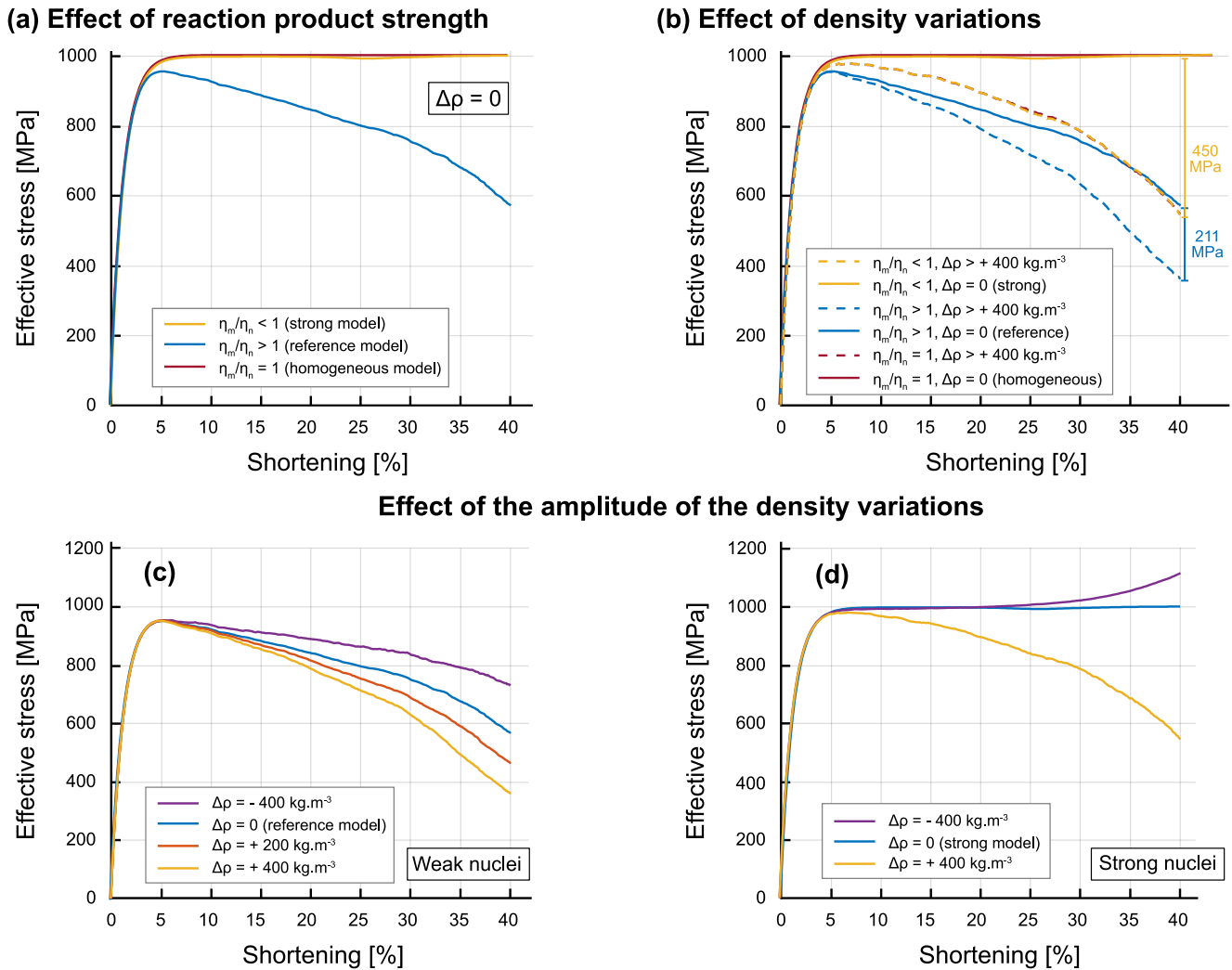


Figure 3. Effect of nuclei strength (a) and density (b–d) on the effective stress of the model. η_m/η_n is the viscosity ratio between the matrix and the nuclei. Panel (b) shows the effect of densification ($\Delta\rho = +400 \text{ kg.m}^{-3}$) on models with stronger nuclei (yellow, model Strong $\Delta\rho\{+400\}$), weaker nuclei (blue, model Weak $\Delta\rho\{+400\}$), and iso-viscous nuclei (purple, model $\Delta\rho\{+400\}$) compared to the matrix. Panels (c) and (d) show the effect of the sign and amplitude of density variations on models with weak nuclei (models Weak $\Delta\rho\{-400\}$, reference, Weak $\Delta\rho\{+200\}$, Weak $\Delta\rho\{+400\}$) and strong nuclei (models Strong $\Delta\rho\{-400\}$, Strong $\Delta\rho\{0\}$, Strong $\Delta\rho\{+400\}$), respectively (see Table 1 for details on the simulations parameters).

be overcome in these areas of the model, which generates a frictional plastic yielding and a resulting weakening. If the difference in density between the matrix and the nuclei is lower than 400 kg.m^{-3} (Weak $\Delta\rho\{+200\}$), the induced weakening is less pronounced (Figure 3c). If the transformation generates a negative density change (Weak $\Delta\rho\{-400\}$), nucleation in the model even reduces the weakening caused by a low viscosity of the nuclei (Figure 3c). In models with strong reaction products, decreasing the density of the nuclei compared to the matrix (Strong $\Delta\rho\{-400\}$) leads to a strengthening of the material (Figure 3d). In that case, the transformation induces an increase of the mean pressure of the model compared to the 2 GPa initial pressure (Figure S5a in Supporting Information S1). Consequently, the material is deformed at conditions further away from the brittle-ductile transition and higher effective stresses are required to reach the yield criterion.

3.5. Evolution of the Model With Work-Driven Nucleation of Weak and Dense Reaction Products (Wd_WD)

As already mentioned in Section 1, nucleation-controlled transformations usually do not result in a uniform distribution of the reaction products in the volume of transforming material. This can be due to several parameters

such as the presence of chemical impurities acting as loci for the nucleation, a heterogeneous distribution of particular grain boundaries that constitute adequate surfaces for nucleation, or a heterogeneous distribution of deformation. Here, we model heterogeneous nucleation in a deformed material through preferential location of the nuclei at places where the mechanical work is the highest (see explanation of the method in Section 2.5). This mechanism is illustrated in Figure S6 in Supporting Information S1. The five inclusions which nucleate between 12.06 and 12.84 hr are indeed located in areas of the model where the total mechanical work (proxy for the strain energy) at the previous step is high. In the following, we will describe the evolution of the Wd_WD model that corresponds to a model with work-driven (Wd) nucleation of nuclei weaker (W) and denser (D) than their matrix (Table 1). Evolution of the accumulated plastic strain over time shows that deformation is more localized in the Wd_WD model than in the reference model (Figure S7c in Supporting Information S1). This is due to the combined effects of densification, that creates several loci of high mechanical work, and work-driven nucleation that takes place at these loci (Figure S6 in Supporting Information S1). The evolution of the Wd_WD model will be used in the following sections as a comparison with models of varying parameters: size of the reaction products, nucleation kinetics, fixed proportions of weak inclusions, and P - $\dot{\epsilon}$ conditions relative to the brittle-ductile transition (Table 1).

3.6. Effect of Work-Driven Nucleation

Results of the model with weak nuclei indicate that work-driven nucleation is responsible for a weakening of the material (Figure 4a). This weakening is more pronounced for the model with no density variations (Wd_W, Table 1), with a strength reduction of more than 300 MPa at 40% shortening (comparison between the blue curves; Figure 4a). However work-driven nucleation adds a strength reduction to the model which is already weakened by the combined effects of viscosity and density variations (100 MPa difference between the orange curves at 40% shortening; Figure 4a).

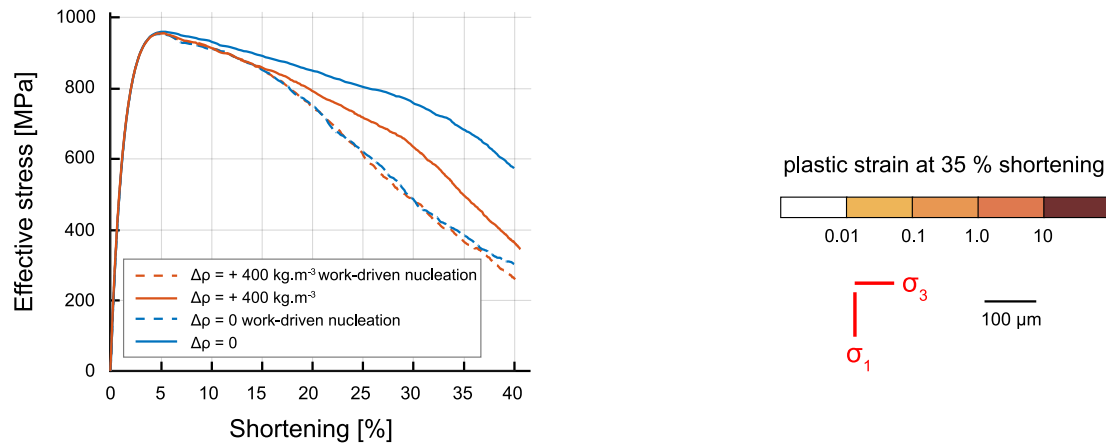
Comparison of the accumulated plastic strain pattern at 35% shortening between models with homogeneous nucleation (reference and Weak $\Delta\rho\{+400\}$; Figures 4b and 4d) and models with work-driven nucleation (Wd_W and Wd_WD; Figures 4c and 4e) shows a more asymmetric distribution of the fractures when the nuclei are preferentially located in domains of high mechanical work. This can also be seen on Figure 5 and Figure S8 in Supporting Information S1 that show instantaneous plastic and viscous strain rates for the four models of Figure 4. Viscous strain rate in the matrix is nearly homogeneous and worth about the value of the background imposed strain rate (10^{-5} s^{-1}). In contrast, viscous strain rate in the nuclei is higher than in the matrix, but while it keeps moderately higher in models without preferential nucleation (Figure 5a and Figure S8a in Supporting Information S1), it increases in areas where viscous shear bands formed through connection of the weak inclusions in models with work-driven nucleation (Figure 5b and Figure S8b in Supporting Information S1). Plastic strain rate is high in the vicinity of the nuclei, along fractures oriented at 45° relative to σ_1 (Figures 5a and 5b; Figure S8a in Supporting Information S1, at 15% shortening). The fracture pattern becomes more asymmetric over time in models Wd_W and Wd_WD (Figure 5b and Figure S8b in Supporting Information S1, at 35% shortening). In models Weak $\Delta\rho\{+400\}$ and Wd_WD, zones of high plastic strain rates form thick bands, characteristics of a high density of fractures (Figure 5b, at 25% shortening and Figure S8a in Supporting Information S1, at 35% shortening). This highlights the contribution of densification in enhancing brittle deformation around the inclusions through a local increase of the stresses (Figure S4c in Supporting Information S1).

Accumulated plastic strain and accumulated viscous strain at 35% shortening in the four models of Figure 4 are displayed in Figure 6. Viscous deformation is concentrated in localized shear bands in models with work-driven nucleation (right panels; Figure 6b) while it is much more distributed in models with random nucleation (left panels; Figure 6b). This is also the case for plastic deformation which is characterized by thicker plastic bands that connect highly deformed inclusions when densification is activated (bottom-right panel; Figure 6a).

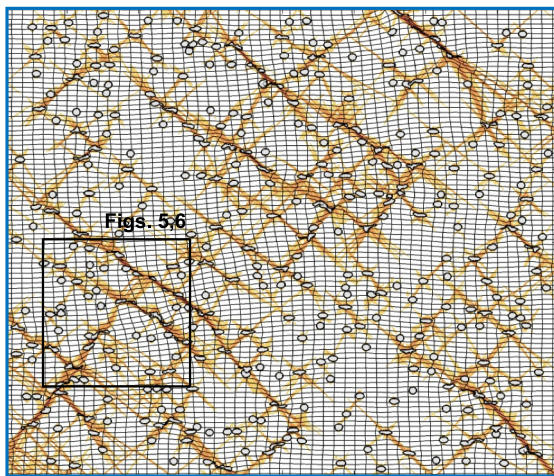
3.7. Effect of the Size of the Reaction Products

In our models, reaction kinetics are modeled by an increase of the reaction extent over time. This reaction extent corresponds to a number of inclusions (nuclei) that nucleates at each time step and depends on the size of the inclusions. In order to maintain constant reaction kinetics between the different simulations, the number of inclusions introduced at each time step is higher if the nuclei are smaller, and lower if the nuclei are bigger. To test the potential effects of nuclei size on the work-driven nucleation pattern and on the mechanical behavior of the

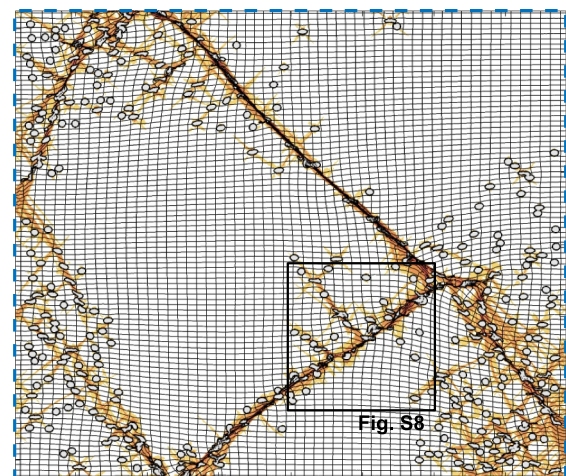
(a) Effect of work-driven nucleation



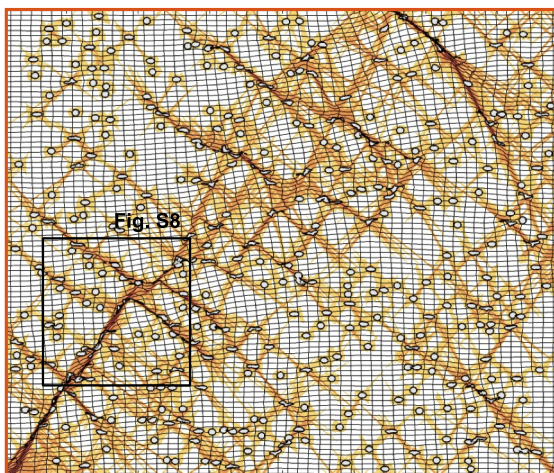
(b) $\Delta\rho = 0$ (reference model)



(c) $\Delta\rho = 0$ + work-driven nucleation



(d) $\Delta\rho = +400 \text{ kg.m}^{-3}$



(e) $\Delta\rho = +400 \text{ kg.m}^{-3}$ + work-driven nucleation (Wd_WD)

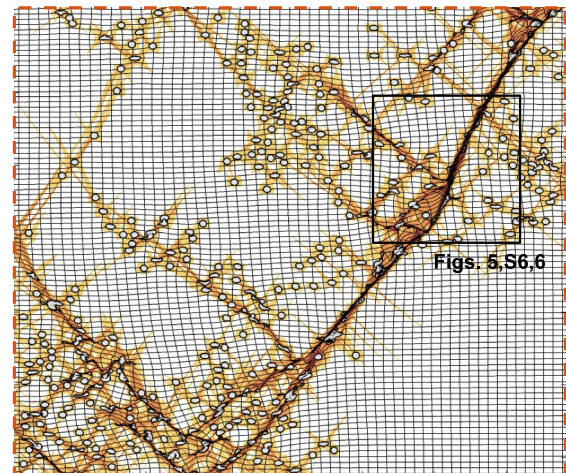


Figure 4. Effect of work-driven nucleation on the effective stress (a) and accumulated plastic strain (b–e) of the models with weak nuclei. Blue curves in (a) are the results of models with no difference in density between the nuclei and their matrix (reference and Wd_W, Table 1). In contrast, orange curves in (a) are the results of models with density variations (Weak $\Delta\rho$ {+400} and Wd_WD, Table 1). Line style of the frame of insets (b–e) is the same as the line style of the corresponding stress-strain curves in (a). Black rectangles indicate the location of the enlargements of Figures 5 and 6; Figures S6 and S8 in Supporting Information S1.

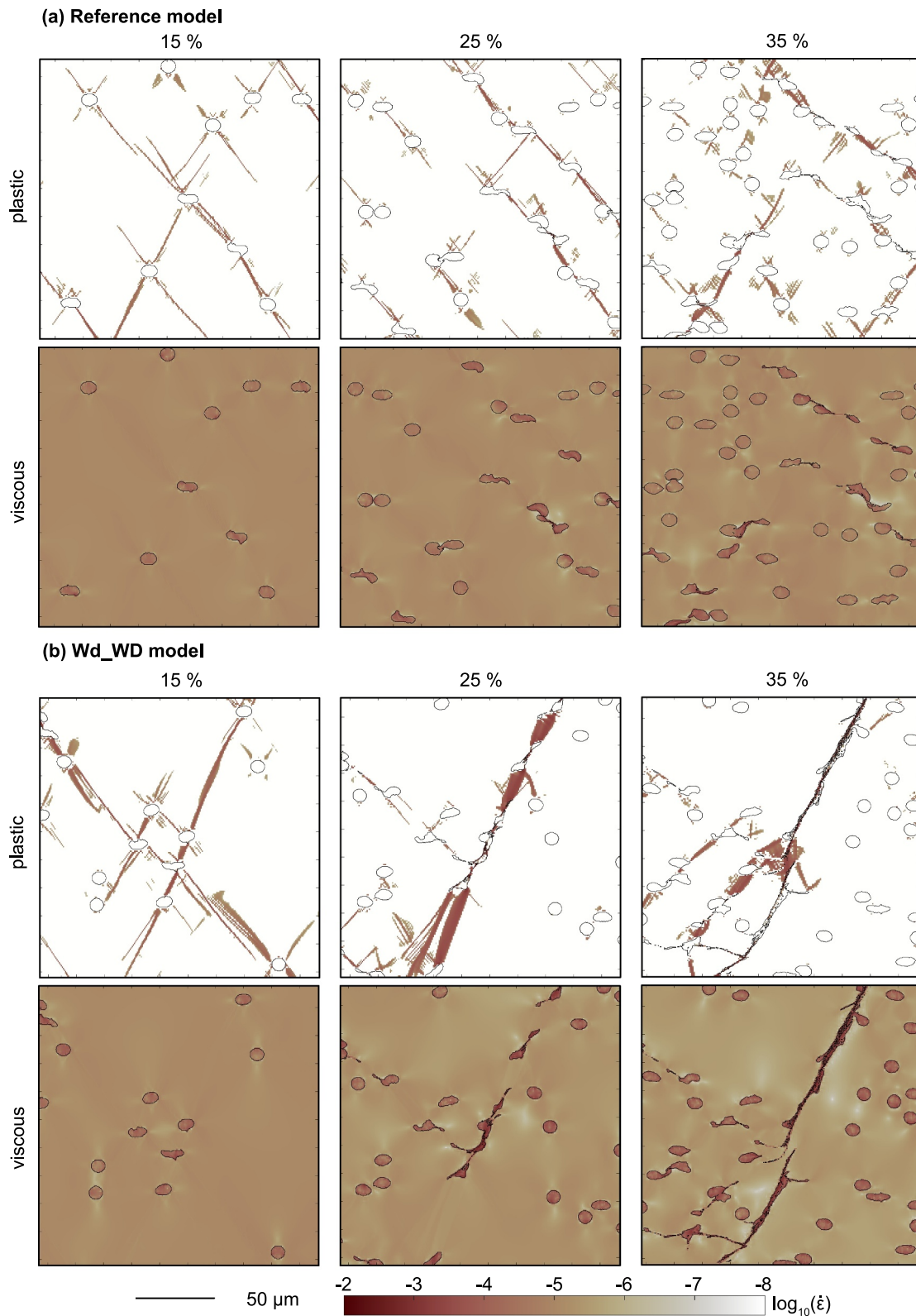


Figure 5. Plastic and viscous strain rates at 15%, 25%, and 35% shortening for (a) the reference model and (b) the Wd_WD model.

(a) Plastic strain at 35 % shortening

(b) Viscous strain at 35 % shortening

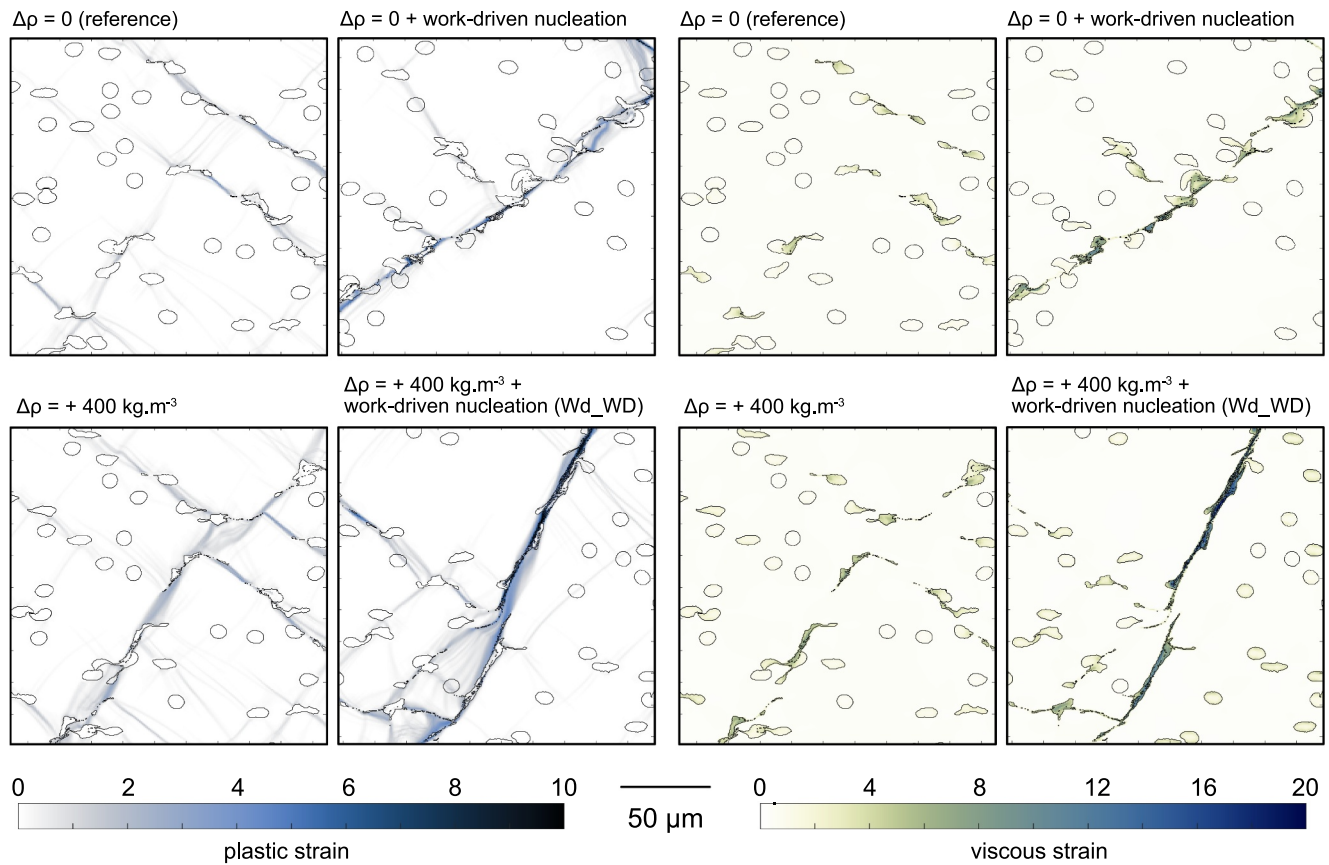


Figure 6. Accumulated plastic strain (a) and viscous strain (b) after 35% shortening for the four models presented in Figure 4 (reference, Wd_W, Weak $\Delta\rho$ {+400} and Wd_WD, Table 1).

material, we compare the results of models designed with nuclei of 5 μm (Wd_WD_5 μm), 10 μm (Wd_WD) and 20 μm (Wd_WD_20 μm) diameter (Figure S9 in Supporting Information S1). Results indicate that models with smaller nuclei are only slightly weaker than models with bigger nuclei.

3.8. Effect of Nucleation Kinetics

A comparison of the results from the Wd_WD model and from a modified Wd_WD model in which nucleation follows kinetics k_1 instead of k_2 (Figure 1b) is presented in Figure 7. The Wd_WD_ k_1 model is characterized by a faster reaction rate than the Wd_WD model (reaction extent of 83% vs. 4.5% at 30% shortening). The behavior of these two models is similar. Indeed, weakening is observed in both models and the rate at which the material weakens mimics the imposed transformation rate (Figure 7a). Effective stress plotted as a function of the reaction progress for both models indicates that reaction kinetics do not have a significant influence on the magnitude of weakening (see the similarity between the curves in Figure 7b), but mainly on the rate of weakening (Figure 7a). At the same amount of shortening, we can see that the reaction extent is much higher for the Wd_WD_ k_1 model ($\sim 15\%$ compared to $\sim 1\%$ in the Wd_WD model) and the deformation is more localized in this model (Figures 7c and 7d).

3.9. Effect of Fixed Proportions of Nuclei

Results from the Wd_WD (kinetics k_2) and the Wd_WD_ k_1 models are compared with those of models that initially contain a certain amount of weak inclusions (5%, 10%, and 20%) that remains constant during the whole simulation (zero kinetics, models X₅, X₁₀ and X₂₀ in Table 1).

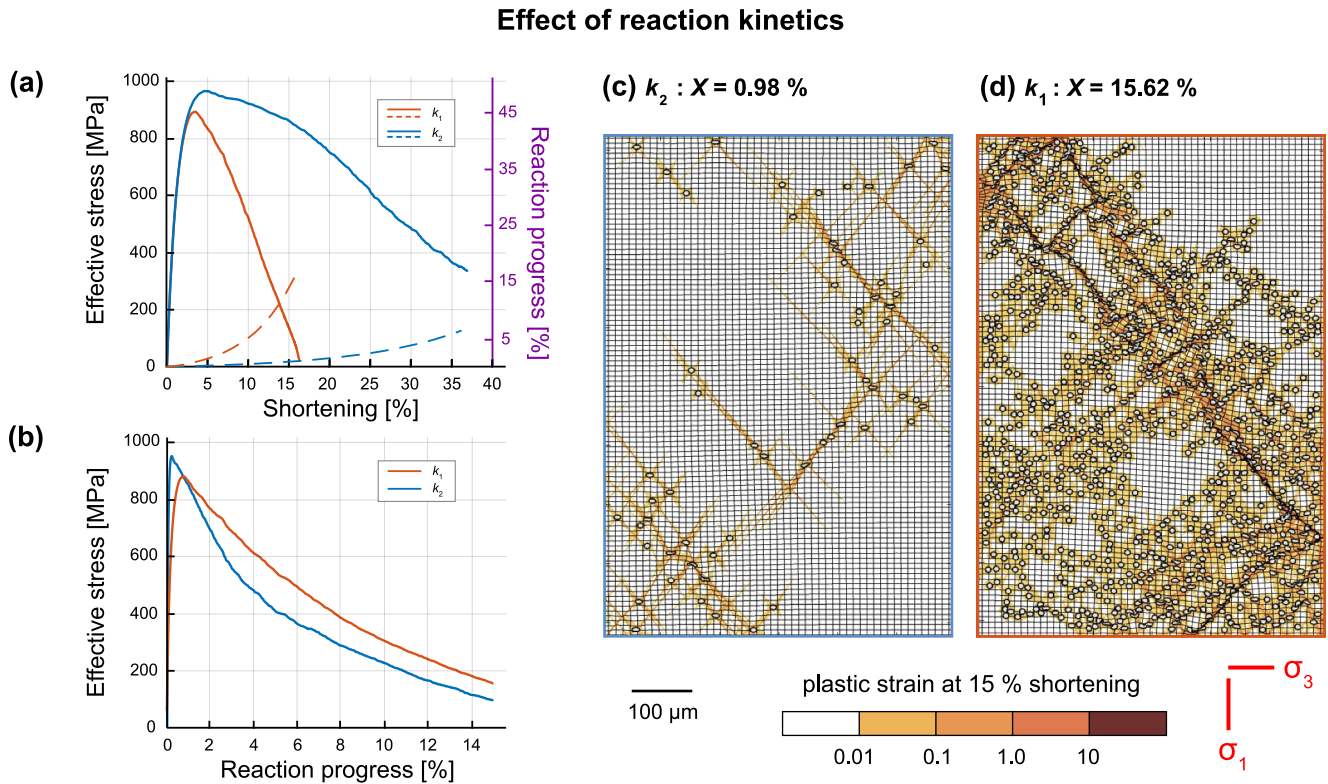


Figure 7. (a) Evolution of the reaction extent for kinetics k_1 and k_2 (dashed lines) and of the effective stress (solid lines) as a function of shortening. (b) Effective stress as a function of the reaction progress. The accumulated plastic strain at 15% shortening is shown in (c) for the Wd_WD model and in (d) for the Wd_WD $_{k_1}$ model.

In models with a fixed proportion of inclusions, weakening is very limited compared to models with nucleation (Figure 8a). The presence of weak inclusions at the beginning of deformation prevents the material from reaching high stresses. In these simulations, weakening begins at $\sim 5\%$ shortening and effective stresses of 750 MPa, 600, and 400 MPa for models X_5 , X_{10} and X_{20} , respectively (Figure 8a). After a weakening of 200 MPa, the effective stresses of these models reach an equilibrium at $\sim 30\%$ shortening, except for the model X_5 which only reaches an equilibrium at 40% shortening (Figure 8b). Models Wd_WD and Wd_WD $_{k_1}$ show both a more pronounced weakening than models with fixed proportions of inclusions, at lower reaction extents. For example, at $\sim 12\%$ shortening, the material in the Wd_WD $_{k_1}$ model is weaker than in the X_{20} model despite having only 9% nuclei (Figure 8a). The same effect can be observed for the Wd_WD model in which the material became (a) weaker than in the X_5 model at 25% shortening when it only contains 2.5% nuclei, (b) weaker than in the X_{10} model at 33% shortening when it only contains 4.7% nuclei and (c) weaker than in the X_{20} model at 40% shortening when it only contains 9.1% nuclei (Figure 8a). This indicates that the mechanism responsible for the weakening observed in models where weak and dense inclusions nucleate in high work domains is more efficient than the mechanism responsible for weakening in the presence of weak inclusions only. A comparison of the accumulated plastic strain patterns of the Wd_WD $_{k_1}$ model, the Wd_WD model and models X_5 , X_{10} and X_{20} at 15%, 25%, and 35% shortening is presented in Figures 7c, 7d, and 8c–8e; Figure S10 in Supporting Information S1. Deformation is more distributed in models with fixed proportions, especially when the initial proportion is high (20% inclusions compared to 5% inclusions). In addition, models with fewer inclusions exhibit a larger proportion of brittle features than models with a higher number of inclusions. This is also the case for models with nucleation in which the material is even more brittle than in the X_5 model. Embrittlement-induced weakening in our models therefore constitutes a more efficient weakening mechanism than the implemented viscous creep.

In models with random location, the material becomes weaker than in fixed proportion models only when the amount of nuclei reaches the amount of inclusions of these fixed proportion models (blue dashed line Figure 8b). In the reference model (no density variations, random nuclei location), an even higher amount of inclusions than in models with fixed proportions is required to reach the same strength (e.g., $X = 13.6\%$ to be weaker than the X_5

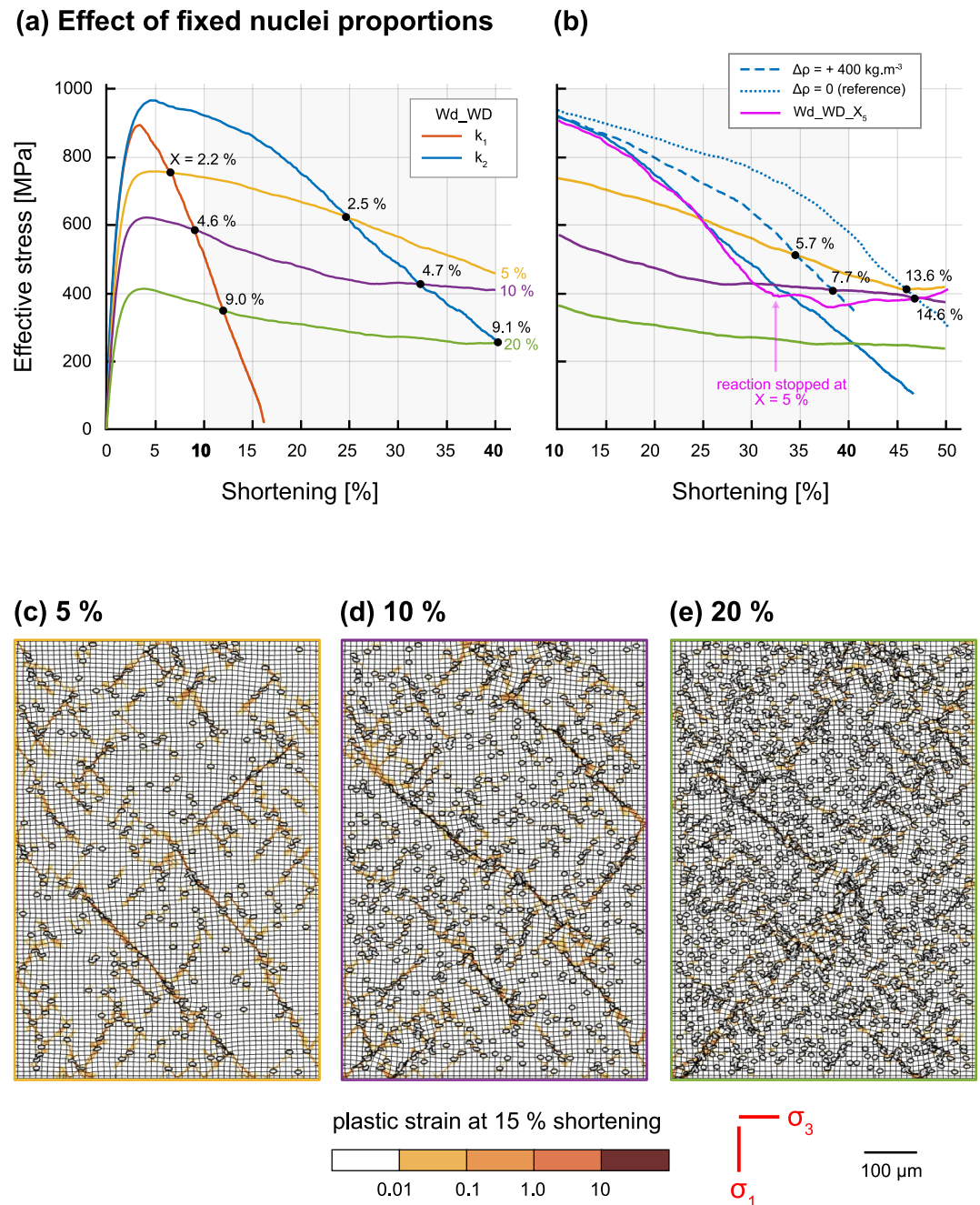


Figure 8. Effect of different initial proportions of weak reaction products (Models X_5 , X_{10} and X_{20}), compared to the models of Figure 7 (kinetics k_1 and k_2). Effective stress as a function of shortening is plotted in (a). Reaction extent for models with kinetics k_1 and k_2 is indicated when their strength reaches that of models with fixed proportions of nuclei (yellow, purple and green lines). Diagram (b) represents the same information as in (a) with only the shortening range between 10% and 50% being shown. Strength evolution of the reference model (blue dashed line) and of the model with nuclei denser than the matrix ($\Delta\rho\{+400\}$; blue dotted line) are represented. In addition, strength evolution of the Wd_WD_ X_5 model where nucleation has been stopped after 5% of reaction is shown for comparison (pink line). Panels (c–e) represent the accumulated plastic strain at 15% shortening for models with 5%, 10%, and 20% of weak nuclei.

model and $X = 14.6\%$ to be weaker than the X_{10} model, blue dotted line Figure 8b). This observation again highlights the dynamics of the weakening induced by (a) densification, and (b) work-driven nucleation. The effect of reaction dynamics is also shown by the evolution of the effective stress of a Wd_WD model where nucleation has been stopped after reaching 5% reaction products (Wd_WD_ X_5 , Table 1; Figure 8b). In this model,

weakening is observed until the transformation stops. The deformed material becomes weaker than in the X_5 model at 25% shortening and 2.5% nuclei, but eventually flows at around 400 MPa, at the same stress level than in the X_5 model after 40% shortening. Note that the stress evolution of this model is not completely identical to that of the Wd_WD model (comparison of blue vs. pink curves; Figure 8b). This is due to the random choice for the position of the nuclei, which is therefore different in these two simulations.

3.10. Effect of the P - $\dot{\epsilon}$ Conditions Relative to the Brittle-Ductile Transition

As mentioned in previous sections, results show that brittle deformation in our models is a more efficient weakening mechanism than viscous deformation. We therefore tested the effect of the P - $\dot{\epsilon}$ conditions relative to the brittle-ductile transition on the mechanical behavior of the material. Figure S11 in Supporting Information S1 presents a comparison between the Wd_WD model (Figure S11c in Supporting Information S1), and two similar models run at (a) 2.5 GPa (i.e., 0.5 GPa above background pressure of the Wd_WD model; Wd_WD_2.5 GPa; Figure S11d in Supporting Information S1), and (b) $\dot{\epsilon} = 10^{-5.5} \text{ s}^{-1}$ (i.e., at lower strain rate than the Wd_WD model; Wd_WD_slow; Figure S11b in Supporting Information S1), respectively. These two models are therefore located further away from the brittle-ductile transition than the Wd_WD model (Figure 1d) and require a higher $\Delta\tau$ to locally reach the plastic yield stress of the material (293 MPa for the model run at 2.5 GPa and 727 MPa for the model run at $10^{-5.5} \text{ s}^{-1}$). As a consequence, the material in the Wd_WD_2.5 GPa model appears stronger than the material of the Wd_WD model during the whole simulation, although it exhibits a similarly pronounced weakening (Figure S11a in Supporting Information S1). Accumulated plastic strain at 40% shortening shows that deformation is slightly more distributed in the Wd_WD_2.5 GPa model than in the model with $P = 2.0$ GPa (Figure S11c and S11d in Supporting Information S1). Material in the Wd_WD_slow model is weaker than in the two other models run at $\dot{\epsilon} = 10^{-5} \text{ s}^{-1}$, due to the matrix itself being weaker. Due to the lower strain rate of this model, it has to be noted that reaction extent is higher than in the Wd_WD model at the same amount of shortening ($X = 9.02\%$ compared to $X = 0.98\%$ at 15% shortening). Accumulated plastic strain in the Wd_WD_slow model shows that plastic deformation has a minor effect on the weakening of the material, which is intrinsically weaker, and that most of the deformation is accumulated by ductile creep of the matrix and its nuclei because the ~ 700 MPa required to fail are rarely reached.

4. Interpretation and Discussion

4.1. Model Limitations

The models presented in this study are based on a two-dimensional discretization of the main equations governing material deformation. As a result, the characteristics of reaction products in the third dimension of space are not taken into account. Cyprych et al. (2016) have proposed an analytical formulation to convert the stresses of two-dimensional numerical models into the stresses that would apply to an equivalent sample deformed in the laboratory (i.e., in three-dimensions). According to this study, the stresses of two-dimensional models considering Newtonian creep (as done in our study) would be 1.33 times higher than those of laboratory experiments. This means that the amount of stress required to reach the yield stress ($\Delta\tau$) would be higher. As this $\Delta\tau$ depends on the amplitude of the densification, the mechanism would remain valid for reaction involving significant densification (e.g., the anorthite breakdown reaction $\Delta\rho \sim 500 \text{ kg}\cdot\text{m}^{-3}$, Zertani et al., 2022). We then expect a less pronounced weakening, similarly to what observed for different values of $\Delta\rho$ (Figure 3).

Additionally, we consider reaction products as circular inclusions although it has been shown that shape and orientation of the inclusions can have an impact on absolute stress levels (Cyprych et al., 2016). In our study however, we focus on the weakening impact and not on the absolute value of the stresses. Therefore, it is relevant to discuss the results of our models in comparison with laboratory experiments from a qualitative point of view (see Section 4.4 and Figure 9), even though our models are only two-dimensional models, and even if reaction products in the laboratory or in nature may be non-spherical, such as zoisite needles formed by plagioclase breakdown at high pressure (Baïssset et al., 2024; Stünitz & Tullis, 2001).

In this study, we consider phases of constant viscosity (i.e., viscosities that do not depend on temperature nor on a stress exponent). This choice was made to study independently the parameters responsible for weakening (inclusion strength, density variations, preferential location of the nuclei). Consequently, the effect of shear-heating on the softening of the material is not taken into account in our models. However, the heat produced by

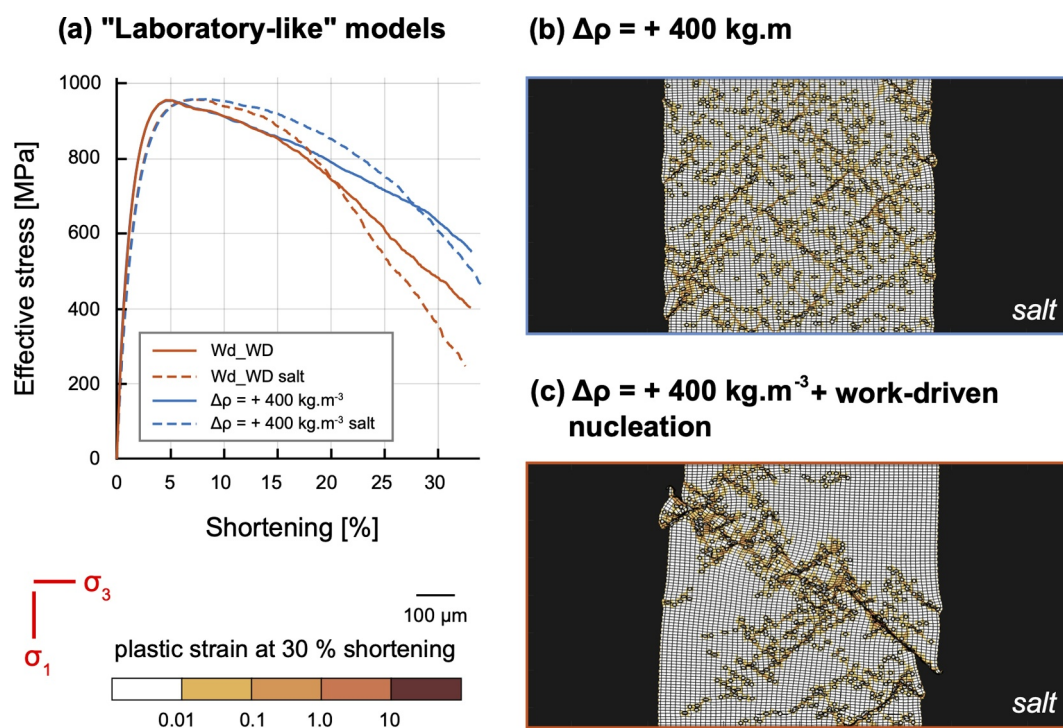


Figure 9. Models of a reacting matrix surrounded by a weak material (here salt) as in laboratory experiments, with salt surrounding the sample. (a) Effective stress in the “matrix-inclusions” system. Accumulated plastic strain (b and c) is shown after 30% shortening.

mechanical processes in our models is negligible (temperature variations $<0.0001^\circ\text{C}$), so it is not relevant to introduce a temperature dependency for viscosity at this scale.

The viscosity of the studied phases is assumed to be Newtonian. If a matrix rheology with a stress exponent $n > 1$ were to be used, this would only amplify the phenomenon of strain localization described in the results. The results of a modified Wd_WD model run with a stress exponent $n = 3$ in the matrix power-law creep are shown in Figure S12 in Supporting Information S1 (Wd_WD $_n$, Table 1). The only effect of this stress exponent is to generate a more pronounced decrease in stress at 20% shortening that correspond to a period of fast sliding in areas of the model where the deformation is localized. Apart from nucleation, we do not introduce other sources of material softening in our models. Friction angle and cohesion therefore always remain constant. This has the advantage of allowing us to study only the strain softening linked to preferential nucleation.

The reaction kinetics in our models are not implemented from the equation of heterogeneous nucleation, that involves thermodynamic parameters such as pressure and temperature, because neither the theory itself nor the constants involved in the few existing equations for geological transformations are quantitatively well constrained (Rubie & Thompson, 1985). Therefore, the effect of reaction overstepping on the nucleation rate is not properly considered in this study. This overstepping could have significantly accelerated nucleation kinetics (Rubie, 1998; Wayte et al., 1989) and is therefore tested in our study through the implementation of faster kinetics (Wd_WD $_k$ model). However, we propose for the first time a model that takes into account the effect of strain-enhanced heterogeneous nucleation, which is of major importance in the case of geological transformations (Holyoke & Tullis, 2006b; Rubie, 1998). Indeed, preferential nucleation in zones of high mechanical work allows to simulate a higher local nucleation rate in areas of the model where deformation has been localized. In nature, these areas could correspond to zones with a high density of dislocation, cracks, twins, etc.

Although we are aware of the limitations of our models, our study has the advantage of isolating the main features of metamorphic transformations that can be responsible for localization of the deformation and weakening of the rocks. We used quantities directly extracted from models (such as the work rate), as well as simple equations, to model nucleation kinetics, a mechanism which theory is poorly defined for the geological transformations studied. This enables us to produce models that are simple enough to understand and isolate the effect of the

different parameters on strength, stress evolution and strain localization in materials, but complex enough to correctly model the studied processes at the first order.

4.2. Importance of Reaction Dynamics for Weakening Mechanisms

Our results indicate that weakening and deformation localization are mainly caused by frictional processes. Transformation-induced density variations generate additional stresses around the nuclei that promote the formation of plastic shear bands (Figure S4 in Supporting Information S1). The presence of weak inclusions in a stressed matrix also generates local stress amplification that can be significant depending on the viscosity contrast and on the inclusion spacing (Feng et al., 2023; Yamato et al., 2022). However, these stresses are not necessarily of the same order of magnitude, nor oriented in the same directions than the stresses generated by volume change (Figure 5 in Yamato et al. (2022)). Combined, these two parameters add up in our models to produce a significant increase of the local stresses (Figure S4c in Supporting Information S1). In some areas, these overstresses are sufficient to reach the plastic yield stress of the material. However, the effects of viscosity and density variations are not identical over time. Stresses related to density variations are instantaneously produced, as soon as the inclusion nucleates in the material, and are then accommodated by deformation of the surrounding matrix (Figure S4b in Supporting Information S1), depending on its rheological properties (Dabrowski et al., 2015). In our models, the Maxwell relaxation time for the matrix is $t_{ve} = 0.34$ hr (Figure S2 in Supporting Information S1). After this characteristic relaxation time, no more stresses related to density variations are produced, as the inclusion does not continue to densify. On the contrary, the production of stresses linked to the difference in strength between the nuclei and their matrix persists over time (Figure S4a in Supporting Information S1), as the inclusions remain weak once they have nucleated in the model and also because growth is not considered in this study. Independently, these two parameters (viscosity and density) are responsible for a weakening of the material with strength reductions of the same order of magnitude (comparison between dotted red line and solid blue line in Figure 3). This is valid for the values $\eta_{matrix}/\eta_{nuclei} = 10^4$ and $\Delta\rho = +400$ kg.m⁻³ chosen to represent transformations with a strong negative volume change (e.g., anorthite + water = zoisite + kyanite + quartz, $\Delta V = -14\%$, $\Delta\rho \sim 500$ kg.m⁻³, Bras et al., 2021; Zertani et al., 2022) and weak reaction products (Stünitz & Tullis, 2001). However, we should keep in mind that while the mechanism responsible for the weakening observed in our models remains valid for different amplitudes of these parameters, the order of magnitude of the strength reduction may vary (e.g., Figure 3c). The mechanism combining viscosity decrease and density increase is responsible for a weakening that is more pronounced than the weakening produced by each of these mechanisms individually (blue dotted curve Figure 3). In other words, a material affected by a densification reaction that produces weak phases weakens more than a material only affected by an increase in density, or only affected by a decrease in viscosity. In addition, our results show that densification can be responsible for a significant weakening even if the reaction products are stronger than their matrix (Figure 3d). In the case of the anorthite breakdown reaction, recent experimental studies showed that zoisite, the principal product of this reaction, is not weaker than plagioclase (Incel et al., 2024). Our results therefore reconcile these experimental observations with evidence from natural rocks that clearly show that this reaction leads to weakening (e.g., Bras et al., 2021).

Nucleation can be responsible for a significant weakening: (a) through the dynamics of density variations over time, and (b) through preferential location of the reaction products in highly deformed zones, in the case of heterogeneous nucleation. In fact, our results show that preferential nucleation alone is sufficient to produce a very significant weakening, and that additional density variations of the nuclei do not cause additional weakening (comparison between dotted curves, Figure 4a). The nucleation of reaction products placed close to each other enhances the propagation of frictional bands from nuclei to nuclei (Figure S4c in Supporting Information S1) and the persistence of high strain rates along these bands where viscous deformation of the inclusions and frictional deformation of the matrix contribute to strain softening (Figure S8 in Supporting Information S1). It is interesting to note that the process responsible for the significant weakening observed is the dynamics of the transformation. Indeed, models deformed with a fixed initial amount of weak inclusions show slight weakening, as they present very few zones where stresses are sufficiently high to reach the yield stress (Figure 8). Again, this result can unify the fact that weakening associated with the zoisite forming reaction after plagioclase has been observed in the field with experimental results that show that zoisite has a strength comparable to that of plagioclase at the same grain size (Incel et al., 2024). Heterogeneous nucleation of very fine-grained reaction products can in itself cause a significant weakening no matter what the strength of the reaction products actually is.

4.3. Implications for the Strength of Reactive Materials

Our results show that the strength of a two-phase material in which one of the phases nucleates over time does not follow a simple Reuss-Voigt or Taylor-Sachs model of phase mixture, but can be much lower than the strength expected for the amount of weak inclusions observed. Indeed, when transformation starts in the already loaded material, the overall strength begins to decrease because of the low viscosity of the nuclei, and tends toward the strength of the weak phase according to a phase mixture model (Figure 4a, at 5% shortening). However, density variations and preferential nucleation induce a faster stress drop than viscosity variations alone (Figure 4a, at 15% shortening). Models with density variations and preferential nucleation eventually reach similar stress levels than models affected by viscosity variations only, but at much lower reaction extent (Figure 8a). In particular, heterogeneous nucleation plays an important role in this phenomenon. Indeed, in models where only density and viscosity variations are activated, stress levels similar to those of models with fixed proportions of inclusions are reached, for a relatively similar amount of weak phases (Figure 8b). We are therefore dealing with a form of “geometric weakening” that is, the connectivity of weak reaction products within initial frictional bands is responsible for the weakening of the material through coalescence of the bands into connected high-strain zones, as already observed in previous experimental, field and numerical studies (Gardner et al., 2017; Gerbi et al., 2016; Handy, 1994; Holyoke & Tullis, 2006c; Mansard et al., 2020).

4.4. Comparison With Transformational Faulting in Laboratory Experiments

In this study, we model the deformation of a reactive material at P - T - $\dot{\epsilon}$ conditions close to those of laboratory experiments that focus on the rheological behavior of reactive aggregates at eclogite facies conditions (Baïssset et al., 2024; Gasc et al., 2022; Incel et al., 2017, 2019, 2020; Shi et al., 2018).

Gasc et al. (2022) have shown that a P - T - $\dot{\epsilon}$ domain exists in which transformational faulting is triggered by the transformation of Ge-olivine into Ge-spinel, a reaction analogous to the olivine-ringwoodite transformation in subducting oceanic slabs. In this range of P - T - $\dot{\epsilon}$ values, samples are initially very strong due to low temperatures and high strain rates. Nucleation in this field is not fast enough to create a completely weak assemblage, but fast enough to trigger dynamic instabilities. These results are very similar to those obtained in our Wd_WD model. Indeed, stress-strain curves of samples deformed at intermediate temperatures show a fast and significant weakening for reaction extents on the order of 20%–30% shortening (Gasc et al., 2022, their samples G16, G22 and G23). This weakening is associated with the formation of macroscopic faults that initiate on spear-shaped fractures at $\sim 45^\circ$ from the shortening direction, where the amount of Ge-spinel is much greater than in the rest of the sample, and where deformation is localized. This mechanism is very similar to the mechanism of preferential nucleation in zones of high mechanical work implemented in our study. Additionally, the authors highlight the importance of the negative volume change of the reaction (8%) and of the latent heat release for (a) the nucleation and propagation of mechanical instabilities, and (b) the local reaction rate increase within these fractures. The processes involved in the transformational faulting observed are therefore comparable to those modeled here.

Other experimental studies have also proposed a similar mechanism to explain the seismicity recorded in continental granulites (Shi et al., 2018) and oceanic lawsonite-blueschists (Incel et al., 2017) when they transform at eclogite facies conditions. For these authors, the coalescence of nanoreactions bands that nucleate in areas where stress concentrations are high (e.g., grain boundaries) eventually leads to the formation of macroscopic shear bands. Two mechanisms that have important consequences for the mechanical weakening observed in our models are also involved in these studies: (a) a negative volume change of the same order of magnitude than in our models (e.g., -10% to -20% for the transformations involved in Shi et al. (2018) compared to the -14% in our study) and (b) a grain size reduction implemented here as low viscosity nuclei.

We did not carry out a parametric study to precisely determine a domain of transformation-induced weakening (a domain analogous to the transformational plasticity field of Gasc et al. (2022)). However, we ran several simulations in which different values of the main controlling parameters (pressure, temperature, strain rate and kinetics) were tested (Figure S11 in Supporting Information S1 and Figure 7). When the strain rate is too low (Figure S11 in Supporting Information S1), deformation in the model occurs far from the brittle-ductile transition of the matrix, which consequently reduces its ductile strength (Figure 1d). The stresses required to reach the plastic yield are therefore only reached in very few places of the model and brittle deformation is limited, making the distribution of the mechanical work more homogeneous. This leads to a more homogeneous distribution of the

reaction products within the model (Figure S11a and S11b in Supporting Information S1). The deformed material flows at low effective stress levels and weakens only slightly. In addition, kinetics is fast in comparison with strain rate (i.e., $\dot{X}/\dot{\epsilon}$ is high) and the large amount of weak phases leads to the formation a connected skeleton that imposes low strength on the overall assembly inhibiting fracturing in the strong matrix. When we move away from the brittle-ductile transition by increasing pressure, that is, without changing the ductile strength of the matrix (Figures 1c and 1d; Figure S11a and S11d in Supporting Information S1), weakening occurs as in the Wd_WD model, but the proportion of frictional zones is lower, and a greater amount of shortening is required before the material eventually weakens. In summary, to generate a significant weakening in our models, the initial matrix must be strong enough to be close to its frictional yield (i.e., at low T and/or fast $\dot{\epsilon}$), and reaction kinetics must be fast enough relative to the strain rate to enhance fracture nucleation through local stress increase between closely spaced nuclei. These results are in agreement with the results of deformation experiments on lower crustal rocks, where slow reaction rates in strong plagioclase aggregates are responsible for weakening. For a specific range of $\dot{X}/\dot{\epsilon}$, this weakening can even be achieved through frictional processes (i.e., embrittlement, Baïssset et al., 2024; Incel et al., 2019; Shi et al., 2018).

A difference between our models and laboratory experiments in which transformational plasticity has been observed is the speed of the stress drop associated with the formation of a frictional band crosscutting the sample. While the fracture pattern described in Gasc et al. (2022) looks very similar the one observed in the Wd_WD model (Figure 4e), the associated stress drop is much faster in their experiments than in our model (Figure 4a). This may be due to the fact that (a) dynamic rupture propagation is not implemented in our models, but fracturing consists of the propagation of plastic shear bands instead, and (b) experimental samples are surrounded by a very soft material (usually NaCl) that allows the two parts of the sample to slip relative to each other, once they have been separated by a fault plane. To tackle this second point, we ran two simulations in which the matrix is surrounded by a soft material (salt), with a viscosity ten times lower than the viscosity of the nuclei (Figure 9). Results show that the rheological behavior of the material is similar in models with and without salt, that is, a stronger weakening is observed in models with controlled location of the nuclei. However, the amplitude of the stress reduction is greater and the stress drop is faster when the matrix is surrounded by salt. Additionally, the difference in strength between simulations ran with or without preferential location of the nuclei (Wd_WD) is greater for the models with salt (Figure 9b vs. Figure 9c). When preferential nucleation is activated in these models, sliding is observed on the main fault plane that crosscut the sample. The geometry of these models is therefore very similar to that of experimental samples, in which reaction and fracture zones are spatially associated (e.g., Figure 9 in Gasc et al. (2022)). This highlights the need for considering the effects on stress variations of an evolving sample geometry when modeling experimental assemblies (Cionoiu et al., 2022).

4.5. Brittle Versus Ductile Deformation

In our models, brittle deformation in the matrix and ductile deformation in the weak nuclei occur simultaneously. Plastic and viscous shear bands interact within zones of high reaction rate where deformation is highly localized. The temporal relationship between ductile shear zones and frictional features (e.g., fractures, pseudotachylytes, breccias) is often an issue for field geologists who observed these two types of deformation patterns coexisting in the same outcrops (Austrheim & Boundy, 1994; Campbell & Menegon, 2019; Hertgen et al., 2017; Jamtveit et al., 2019; John & Schenk, 2006; John et al., 2009; Lund & Austrheim, 2003; Scambelluri et al., 2017; Scholz & Choi, 2022; Steltenpohl et al., 2006). Several studies, both natural and experimental, have proposed that ductile shear zones initiate on pre-existing faults (Incel et al., 2020; Mancktelow & Pennacchioni, 2005; Menegon et al., 2017; Segall & Simpson, 1986; Tullis et al., 1990). Similarly, fracturing in our models produces a mechanical work that enhances local high nucleation rates of weak reaction products. Viscous shear zones then localize on this products, overprinting the plastic bands. It is also often proposed that frictional bands in nature promote the circulation of fluids that would then be responsible for an increase of reaction kinetics. Therefore, although fluid flow is not implemented in our models, the mechanism of work-driven nucleation well describes the interplay between enhanced nucleation and frictional bands. Implementing fluid flow would only contribute to this process. Eventually, once a main localized ductile zone has formed in our models, nucleation continues everywhere in the matrix, generating new brittle zones. This could be regarded as brittle-ductile cycles similar to those described in several studies based on field observations (Giuntoli & Viola, 2021; Hawemann et al., 2019; Menegon et al., 2021; Rogowitz et al., 2024).

5. Conclusion

We presented here a series of numerical models that provide valuable insights on the role of reaction dynamics on rock rheology. The interplay between deformation and transformation at high pressure is addressed by implementing the nucleation of inclusions, denser and weaker than their matrix, which are preferentially placed in domains of high mechanical work. Our results show that weakening of the rocks is not just a matter of the strength of the newly formed reaction products. Indeed, a significant decrease in density can generate a transient weakening of the material even if the reaction products are stronger than their matrix, as density variations control the background pressure and the state of stress of the system. Locally, these variations in stress and pressure allow reaching the plastic yield stress of the matrix. The resulting initiation and coalescence of fractures are then responsible for strain localization and weakening of the material. In addition, our results indicate that preferential nucleation of weak inclusions in highly strained zones (plastic and ductile) has an even more significant impact on the mechanical behavior of the material than viscosity and density variations alone. Eventually, results show that weakening is a dynamic process controlled by reaction kinetics rather than reaction extent as it depends on (a) the difference between the physical properties of the matrix and those of the reaction products (viscosity and density), and (b) the nucleation style (heterogeneous vs. homogeneous). We show that transformational weakening in reactive materials through fracture nucleation and coalescence requires (a) a state of stress close to the brittle-ductile transition (involving low temperatures or fast strain rates) and (b) a fast reaction rate relative to the strain rate, in line with previous results from laboratory experiments. Our study therefore provides new perspectives for the numerical modeling of two dynamic processes that occurs simultaneously in nature: metamorphic transformations and rock deformation.

Data Availability Statement

The data of this study have been generated by using the code MDoodz6.0. This code is freely accessible and all the information needed to install the code and use it is available through Zenodo (Baïssset et al., 2024a), including the updated files of the code specifically written for this study (with work computation and nucleation routines). The Matlab file used to read the Output files and produce the figures of this paper is also given (Baïssset et al., 2024a). In addition, Output data are provided for both the reference model (Baïssset et al., 2024b) and the Wd_WD model (Baïssset et al., 2024c). Movies of the evolution of the accumulated plastic strain for all the simulations listed in Table 1 are provided (Baïssset et al., 2024d).

Acknowledgments

This work was conducted as part of the project METROLOGY supported by the ANR (ANR-23-CE49-0008). It has also benefited from previous IUF financial support to P.Y. that partly financed the purchase of the computing nodes used for numerical simulations. Scientific discussions between the authors was also highly facilitated by the Heraeus Foundation endowed visiting professorship to P.Y. at the Institute of Geosciences of Goethe University Frankfurt (Frankfurt am Main, Germany). We thank S. Zertani and an anonymous reviewer for their very constructive suggestions that truly helped us to improve the manuscript.

References

- Alvizuri, C., & Hetényi, G. (2019). Source mechanism of a lower crust earthquake beneath the himalayas and its possible relation to metamorphism. *Tectonophysics*, 769, 128153. <https://doi.org/10.1016/j.tecto.2019.06.023>
- Austrheim, H., & Boundy, T. (1994). Pseudotachylytes generated during seismic faulting and eclogitization of the deep crust. *Science*, 265(5168), 82–83. <https://doi.org/10.1126/science.265.5168.82>
- Avrami, M. (1939). Kinetics of phase change. I General theory. *The Journal of Chemical Physics*, 7(12), 1103–1112. <https://doi.org/10.1063/1.1750380>
- Baïssset, M., Labrousse, L., Schubnel, A., Gasc, J., Béneut, K., & Guillaumet, M. (2024). Rheology of hydrated plagioclase at lower crustal conditions: Cataclasis, creep and transformational plasticity. *Journal of Structural Geology*, 178, 105010. <https://doi.org/10.1016/j.jsg.2023.105010>
- Baïssset, M., Labrousse, L., Yamato, P., & Schubnel, A. (2023). Twinning and partial melting as early weakening processes in plagioclase at high pressure: Insights from Holsnøy (Scandinavian Caledonides, Norway). *Contributions to Mineralogy and Petrology*, 178(3), 19. <https://doi.org/10.1007/s00410-023-01998-x>
- Baïssset, M., Yamato, P., & Duretz, T. (2024a). Files relative to MDoodz6.0 code used in Baïssset et al. paper entitled “Weakening induced by phase nucleation in metamorphic rocks: Insights from numerical models” [Software]. *Zenodo*. <https://doi.org/10.5281/zenodo.13871879>
- Baïssset, M., Yamato, P., & Duretz, T. (2024b). Output files of the reference model from Baïssset et al. paper entitled “Weakening induced by phase nucleation in metamorphic rocks: Insights from numerical models” [Dataset]. *Zenodo*. <https://doi.org/10.5281/zenodo.11475337>
- Baïssset, M., Yamato, P., & Duretz, T. (2024c). Output files of the WDSE model from Baïssset et al. paper entitled “Weakening induced by phase nucleation in metamorphic rocks: Insights from numerical models” [Dataset]. *Zenodo*. <https://doi.org/10.5281/zenodo.11477924>
- Baïssset, M., Yamato, P., & Duretz, T. (2024d). Movies of the simulations performed in Baïssset et al. paper entitled “Weakening induced by phase nucleation in metamorphic rocks: Insights from numerical models” [Dataset]. *Zenodo*. <https://doi.org/10.5281/zenodo.13889673>
- Beall, A., Fagereng, Å., & Ellis, S. (2019). Strength of strained two-phase mixtures: Application to rapid creep and stress amplification in subduction zone mélange. *Geophysical Research Letters*, 46(1), 169–178. <https://doi.org/10.1029/2018gl081252>
- Boullier, A., & Gueguen, Y. (1975). SP-mylonites: Origin of some mylonites by superplastic flow. *Contributions to Mineralogy and Petrology*, 50(2), 93–104. <https://doi.org/10.1007/bf00373329>
- Boundy, T., Fountain, D., & Austrheim, H. (1992). Structural development and petrofabrics of eclogite facies shear zones, Bergen Arcs, western Norway: Implications for deep crustal deformational processes. *Journal of Metamorphic Geology*, 10(2), 127–146. <https://doi.org/10.1111/j.1525-1314.1992.tb00075.x>

- Brantut, N., Schubnel, A., David, E., Héripré, E., Gueguen, Y., & Dimanov, A. (2012). Dehydration-induced damage and deformation in gypsum and implications for subduction zone processes. *Journal of Geophysical Research*, *117*(B3). <https://doi.org/10.1029/2011jb008730>
- Bras, E., Baïssset, M., Yamato, P., & Labrousse, L. (2021). Transient weakening during the granulite to eclogite transformation within hydrous shear zones (Holsnøy, Norway). *Tectonophysics*, *819*, 229026. <https://doi.org/10.1016/j.tecto.2021.229026>
- Brodie, K., & Rutter, E. (1985). On the relationship between deformation and metamorphism, with special reference to the behavior of basic rocks. In *Metamorphic reactions* (pp. 138–179). Springer.
- Brodie, K., & Rutter, E. (2000). Rapid stress release caused by polymorphic transformation during the experimental deformation of quartz. *Geophysical Research Letters*, *27*(19), 3089–3092. <https://doi.org/10.1029/2000gl008505>
- Burnley, P., & Green, H. (1989). Stress dependence of the mechanism of the olivine–spinel transformation. *Nature*, *338*(6218), 753–756. <https://doi.org/10.1038/338753a0>
- Burnley, P., Green, H. W., & Prior, D. J. (1991). Faulting associated with the olivine to spinel transformation in Mg₂GeO₄ and its implications for deep-focus earthquakes. *Journal of Geophysical Research*, *96*(B1), 425–443. <https://doi.org/10.1029/90jb01937>
- Cahn, J. W. (1957). Nucleation on dislocations. *Acta Metallurgica*, *5*(3), 169–172. [https://doi.org/10.1016/0001-6160\(57\)90021-4](https://doi.org/10.1016/0001-6160(57)90021-4)
- Campbell, L., & Menegon, L. (2019). Transient high strain rate during localized viscous creep in the dry lower continental crust (Lofoten, Norway). *Journal of Geophysical Research: Solid Earth*, *124*(10), 10240–10260. <https://doi.org/10.1029/2019jb018052>
- Chen, S., Hiraga, T., & Kohlstedt, D. L. (2006). Water weakening of clinopyroxene in the dislocation creep regime. *Journal of Geophysical Research*, *111*(B8), B08203. <https://doi.org/10.1029/2005jb003885>
- Cionoiu, S., Moulas, E., Stünitz, H., & Tajčmanová, L. (2022). Locally resolved stress-state in samples during experimental deformation: Insights into the effect of stress on mineral reactions. *Journal of Geophysical Research: Solid Earth*, *127*(8), e2022JB024814. <https://doi.org/10.1029/2022jb024814>
- Cyprich, D., Brune, S., Piazzolo, S., & Quinteros, J. (2016). Strain localization in polycrystalline material with second phase particles: Numerical modeling with application to ice mixtures. *Geochemistry, Geophysics, Geosystems*, *17*(9), 3608–3628. <https://doi.org/10.1002/2016gc006471>
- Dabrowski, M., Powell, R., & Podladchikov, Y. (2015). Viscous relaxation of grain-scale pressure variations. *Journal of Metamorphic Geology*, *33*(8), 859–868. <https://doi.org/10.1111/jmg.12142>
- Dabrowski, M., Schmid, D., & Podladchikov, Y. (2012). A two-phase composite in simple shear: Effective mechanical anisotropy development and localization potential. *Journal of Geophysical Research*, *117*(B8), B08406. <https://doi.org/10.1029/2012jb009183>
- De Ronde, A., Heilbronner, R., Stünitz, H., & Tullis, J. (2004). Spatial correlation of deformation and mineral reaction in experimentally deformed plagioclase–olivine aggregates. *Tectonophysics*, *389*(1–2), 93–109. <https://doi.org/10.1016/j.tecto.2004.07.054>
- De Ronde, A., Stünitz, H., Tullis, J., & Heilbronner, R. (2005). Reaction-induced weakening of plagioclase–olivine composites. *Tectonophysics*, *409*(1–4), 85–106. <https://doi.org/10.1016/j.tecto.2005.08.008>
- Dimanov, A., & Dresen, G. (2005). Rheology of synthetic anorthite–diopside aggregates: Implications for ductile shear zones. *Journal of Geophysical Research*, *110*(B7), B07203. <https://doi.org/10.1029/2004jb003431>
- Dobson, D., Meredith, P., & Boon, S. (2002). Microseismicity associated with antigorite dehydration: Laboratory simulation of deep-focus earthquakes. In *EGS General Assembly Conference Abstracts* (p. 3985).
- Dunand, D. C., Schuh, C., & Goldsby, D. L. (2001). Pressure-induced transformation plasticity of H₂O ice. *Physical Review Letters*, *86*(4), 668–671. <https://doi.org/10.1103/physrevlett.86.668>
- Duret, T., de Borst, R., & Yamato, P. (2021). Modeling lithospheric deformation using a compressible visco-elasto-viscoplastic rheology and the effective viscosity approach. *Geochemistry, Geophysics, Geosystems*, *22*(8), e2021GC009675. <https://doi.org/10.1029/2021gc009675>
- Duret, T., de Borst, R., Yamato, P., & Le Pourhiet, L. (2020). Toward robust and predictive geodynamic modeling: The way forward in frictional plasticity. *Geophysical Research Letters*, *47*(5), e2019GL086027. <https://doi.org/10.1029/2019gl086027>
- Feng, H., Gerbi, C. C., & Johnson, S. E. (2023). Numerical exploration of factors that control stress amplification in Earth's lithosphere. *Geophysical Journal International*, *235*(3), 2927–2947. <https://doi.org/10.1093/gji/ggad394>
- Ferrand, T. P., Hilairet, N., Incel, S., Deldicque, D., Labrousse, L., Gasc, J., et al. (2017). Dehydration-driven stress transfer triggers intermediate-depth earthquakes. *Nature Communications*, *8*(1), 1–11. <https://doi.org/10.1038/ncomms15247>
- Furusho, M., & Kanagawa, K. (1999). Transformation-induced strain localization in a lherzolite mylonite from the Hidaka metamorphic belt of central Hokkaido, Japan. *Tectonophysics*, *313*(4), 411–432. [https://doi.org/10.1016/s0040-1951\(99\)00215-2](https://doi.org/10.1016/s0040-1951(99)00215-2)
- Gaidies, F. (2017). Nucleation in geological materials. *EMU Notes in Mineralogy*, *16*, 347–371. <https://doi.org/10.1180/emu-notes.16.11>
- Gaidies, F., Pattison, D., & De Capitani, C. (2011). Toward a quantitative model of metamorphic nucleation and growth. *Contributions to Mineralogy and Petrology*, *162*(5), 975–993. <https://doi.org/10.1007/s00410-011-0635-2>
- Gardner, R., Piazzolo, S., Evans, L., & Daczko, N. (2017). Patterns of strain localization in heterogeneous, polycrystalline rocks—A numerical perspective. *Earth and Planetary Science Letters*, *463*, 253–265. <https://doi.org/10.1016/j.epsl.2017.01.039>
- Gasc, J., Gardonio, B., Deldicque, D., Daigre, C., Moarefvand, A., Petit, L., et al. (2022). Ductile vs. brittle strain localization induced by the olivine–ringwoodite transformation. *Minerals*, *12*(6), 719. <https://doi.org/10.3390/min12060719>
- Gerald, J. F., & Stünitz, H. (1993). Deformation of granulites at low metamorphic grade. I: Reactions and grain size reduction. *Tectonophysics*, *221*(3–4), 269–297. [https://doi.org/10.1016/0040-1951\(93\)90163-e](https://doi.org/10.1016/0040-1951(93)90163-e)
- Gerbi, C., Johnson, S. E., Shulman, D., & Klepeis, K. (2016). Influence of microscale weak zones on bulk strength. *Geochemistry, Geophysics, Geosystems*, *17*(10), 4064–4077. <https://doi.org/10.1002/2016gc006551>
- Gerya, T. V., & Yuen, D. A. (2003). Characteristics-based marker-in-cell method with conservative finite-differences schemes for modeling geological flows with strongly variable transport properties. *Physics of the Earth and Planetary Interiors*, *140*(4), 293–318. <https://doi.org/10.1016/j.pepi.2003.09.006>
- Giuntoli, F., Menegon, L., & Warren, C. J. (2018). Replacement reactions and deformation by dissolution and precipitation processes in amphibolites. *Journal of Metamorphic Geology*, *36*(9), 1263–1286. <https://doi.org/10.1111/jmg.12445>
- Giuntoli, F., & Viola, G. (2021). Cyclic brittle-ductile oscillations recorded in exhumed high-pressure continental units: A record of deep episodic tremor and slow slip events in the northern Apennines. *Geochemistry, Geophysics, Geosystems*, *22*(9), e2021GC009805. <https://doi.org/10.1029/2021gc009805>
- Gueydan, F., Leroy, Y. M., Jolivet, L., & Agard, P. (2003). Analysis of continental midcrustal strain localization induced by microfracturing and reaction-softening. *Journal of Geophysical Research*, *108*(B2), 2064. <https://doi.org/10.1029/2001jb000611>
- Hacker, B. R., Peacock, S. M., Abers, G. A., & Holloway, S. D. (2003). Subduction factory 2. Are intermediate-depth earthquakes in subducting slabs linked to metamorphic dehydration reactions? *Journal of Geophysical Research*, *108*(B1), 2030. <https://doi.org/10.1029/2001jb001129>
- Handy, M. (1989). Deformation regimes and the rheological evolution of fault zones in the lithosphere: The effects of pressure, temperature, grain size and time. *Tectonophysics*, *163*(1–2), 119–152. [https://doi.org/10.1016/0040-1951\(89\)90122-4](https://doi.org/10.1016/0040-1951(89)90122-4)

- Handy, M. (1994). Flow laws for rocks containing two non-linear viscous phases: A phenomenological approach. *Journal of Structural Geology*, 16(3), 287–301. [https://doi.org/10.1016/0191-8141\(94\)90035-3](https://doi.org/10.1016/0191-8141(94)90035-3)
- Handy, M., & Stünitz, H. (2002). Strain localization by fracturing and reaction weakening—A mechanism for initiating exhumation of subcontinental mantle beneath rifted margins. *Geological Society, London, Special Publications*, 200(1), 387–407. <https://doi.org/10.1144/gsl.sp.2001.200.01.22>
- Hawemann, F., Mancktelow, N. S., Pennacchioni, G., Wex, S., & Camacho, A. (2019). Weak and slow, strong and fast: How shear zones evolve in a dry continental crust (Musgrave Ranges, Central Australia). *Journal of Geophysical Research: Solid Earth*, 124(1), 219–240. <https://doi.org/10.1029/2018jb016559>
- Hertgen, S., Yamato, P., Morales, L. F., & Angiboust, S. (2017). Evidence for brittle deformation events at eclogite-facies PT conditions (example of the Mt. Emilius klippe, Western Alps). *Tectonophysics*, 706, 1–13. <https://doi.org/10.1016/j.tecto.2017.03.028>
- Hetényi, G., Cattin, R., Brunet, F., Bollinger, L., Vergne, J., Nábělek, J. L., & Diament, M. (2007). Density distribution of the India plate beneath the Tibetan plateau: Geophysical and petrological constraints on the kinetics of lower-crustal eclogitization. *Earth and Planetary Science Letters*, 264(1–2), 226–244. <https://doi.org/10.1016/j.epsl.2007.09.036>
- Hidas, K., Garrido, C. J., Tommasi, A., Padrón-Navarta, J. A., Thielmann, M., Konc, Z., et al. (2013). Strain localization in pyroxenite by reaction-enhanced softening in the shallow subcontinental lithospheric mantle. *Journal of Petrology*, 54(10), 1997–2031. <https://doi.org/10.1093/petrology/egt039>
- Holyoke, C. W., & Tullis, J. (2006a). Formation and maintenance of shear zones. *Geology*, 34(2), 105–108. <https://doi.org/10.1130/g22116.1>
- Holyoke, C. W., & Tullis, J. (2006b). The interaction between reaction and deformation: An experimental study using a biotite+ plagioclase+ quartz gneiss. *Journal of Metamorphic Geology*, 24(8), 743–762. <https://doi.org/10.1111/j.1525-1314.2006.00666.x>
- Holyoke, C. W., & Tullis, J. (2006c). Mechanisms of weak phase interconnection and the effects of phase strength contrast on fabric development. *Journal of Structural Geology*, 28(4), 621–640. <https://doi.org/10.1016/j.jsg.2006.01.008>
- Incel, S., Baïssat, M., Labrousse, L., & Schubnel, A. (2023). Partial melting and reaction along deformation features in plagioclase. *Journal of Metamorphic Geology*, 41(3), 449–464. <https://doi.org/10.1111/jmg.12702>
- Incel, S., Hilairet, N., Labrousse, L., John, T., Deldicque, D., Ferrand, T., et al. (2017). Laboratory earthquakes triggered during eclogitization of lawsonite-bearing blueschist. *Earth and Planetary Science Letters*, 459, 320–331. <https://doi.org/10.1016/j.epsl.2016.11.047>
- Incel, S., Labrousse, L., Hilairet, N., John, T., Gasc, J., Shi, F., et al. (2019). Reaction-induced embrittlement of the lower continental crust. *Geology*, 47(3), 235–238. <https://doi.org/10.1130/g45527.1>
- Incel, S., Mohrbach, L. K., & Renner, J. (2024). How strong/weak is epidote relative to plagioclase? *Geochemistry, Geophysics, Geosystems*, 25(2), e2023GC011275. <https://doi.org/10.1029/2023gc011275>
- Incel, S., Renner, J., & Jamtveit, B. (2020). Evolution of brittle structures in plagioclase-rich rocks at high-pressure and high-temperature conditions—Linking laboratory results to field observations. *Geochemistry, Geophysics, Geosystems*, 21(8), e2020GC009028. <https://doi.org/10.1029/2020gc009028>
- Jamtveit, B., Petley-Ragan, A., Incel, S., Dunkel, K. G., Aupart, C., Austrheim, H., et al. (2019). The effects of earthquakes and fluids on the metamorphism of the lower continental crust. *Journal of Geophysical Research: Solid Earth*, 124(8), 7725–7755. <https://doi.org/10.1029/2018jb016461>
- Jaumann, G. (1911). Geschlossenes System physikalischer und chemischer Differentialgesetze. *Sitzber. Akad. Wiss. Wien (IIa)*, 120, 385.
- Jessell, M. W., Bons, P. D., Griera, A., Evans, L. A., & Wilson, C. J. (2009). A tale of two viscosities. *Journal of Structural Geology*, 31(7), 719–736. <https://doi.org/10.1016/j.jsg.2009.04.010>
- Ji, S., Wang, Z., & Wirth, R. (2001). Bulk flow strength of forsterite–enstatite composites as a function of forsterite content. *Tectonophysics*, 341(1–4), 69–93. [https://doi.org/10.1016/s0040-1951\(01\)00191-3](https://doi.org/10.1016/s0040-1951(01)00191-3)
- Jin, Z.-M., Zhang, J., Green, H., & Jin, S. (2001). Eclogite rheology: Implications for subducted lithosphere. *Geology*, 29(8), 667–670. [https://doi.org/10.1130/0091-7613\(2001\)029<0667:erifsl>2.0.co;2](https://doi.org/10.1130/0091-7613(2001)029<0667:erifsl>2.0.co;2)
- John, T., Medvedev, S., Rüpke, L. H., Andersen, T. B., Podladchikov, Y. Y., & Austrheim, H. (2009). Generation of intermediate-depth earthquakes by self-localizing thermal runaway. *Nature Geoscience*, 2(2), 137–140. <https://doi.org/10.1038/ngeo419>
- John, T., & Schenk, V. (2006). Interrelations between intermediate-depth earthquakes and fluid flow within subducting oceanic plates: Constraints from eclogite facies pseudotachylytes. *Geology*, 34(7), 557–560. <https://doi.org/10.1130/g22411a.1>
- Johnson, S. E., Song, W. J., Cook, A. C., Vel, S. S., & Gerbi, C. C. (2021). The quartz $\alpha \leftrightarrow \beta$ phase transition: Does it drive damage and reaction in continental crust? *Earth and Planetary Science Letters*, 553, 116622. <https://doi.org/10.1016/j.epsl.2020.116622>
- Jung, H., Green II, H. W., & Dobrzynetskaia, L. F. (2004). Intermediate-depth earthquake faulting by dehydration embrittlement with negative volume change. *Nature*, 428(6982), 545–549. <https://doi.org/10.1038/nature02412>
- Kelemen, P. B., & Hirth, G. (2012). Reaction-driven cracking during retrograde metamorphism: Olivine hydration and carbonation. *Earth and Planetary Science Letters*, 345, 81–89. <https://doi.org/10.1016/j.epsl.2012.06.018>
- Keller, L., Abart, R., Stünitz, H., & De Capitani, C. (2004). Deformation, mass transfer and mineral reactions in an eclogite facies shear zone in a polymetamorphic metapelite (Monte Rosa nappe, western Alps). *Journal of Metamorphic Geology*, 22(2), 97–118. <https://doi.org/10.1111/j.1525-1314.2004.00500.x>
- Kenkmann, T., & Dresen, G. (2002). Dislocation microstructure and phase distribution in a lower crustal shear zone—an example from the Ivrea-Zone, Italy. *International Journal of Earth Sciences*, 91(3), 445–458. <https://doi.org/10.1007/s00531-001-0236-9>
- Kerrich, R., Allison, I., Barnett, R. L., Moss, S., & Starkey, J. (1980). Microstructural and chemical transformations accompanying deformation of granite in a shear zone at Mieville, Switzerland; with implications for stress corrosion cracking and superplastic flow. *Contributions to Mineralogy and Petrology*, 73(3), 221–242. <https://doi.org/10.1007/bf00381442>
- Ketcham, R., & Carlson, W. (2012). Numerical simulation of diffusion-controlled nucleation and growth of porphyroblasts. *Journal of Metamorphic Geology*, 30(5), 489–512. <https://doi.org/10.1111/j.1525-1314.2012.00978.x>
- Kirby, S. H., Stein, S., Okal, E. A., & Rubie, D. (1996). Metastable mantle phase transformations and deep earthquakes in subducting oceanic lithosphere. *Reviews of Geophysics*, 34(2), 261–306. <https://doi.org/10.1029/96rg01050>
- Klaper, E. M. (1990). Reaction-enhanced formation of eclogite-facies shear zones in granulite-facies anorthositic. *Geological Society, London, Special Publications*, 54(1), 167–173. <https://doi.org/10.1144/gsl.sp.1990.054.01.16>
- Kohlstedt, D. L. (2006). The role of water in high-temperature rock deformation. *Reviews in Mineralogy and Geochemistry*, 62(1), 377–396. <https://doi.org/10.2138/rmg.2006.62.16>
- Kronenberg, A. K., Segall, P., & Wolf, G. H. (1990). Hydrolytic weakening and penetrative deformation within a natural shear zone. *The Brittle-Ductile Transition in Rocks*, 56, 21–36. <https://doi.org/10.1029/gm056p0021>
- Luisier, C., Tajčmanová, L., Yamato, P., & Duret, T. (2023). Garnet microstructures suggest ultra-fast decompression of ultrahigh-pressure rocks. *Nature Communications*, 14(1), 6012. <https://doi.org/10.1038/s41467-023-41310-w>

- Lund, M. G., & Austrheim, H. (2003). High-pressure metamorphism and deep-crustal seismicity: Evidence from contemporaneous formation of pseudotachylytes and eclogite facies coronas. *Tectonophysics*, 372(1–2), 59–83. [https://doi.org/10.1016/s0040-1951\(03\)00232-4](https://doi.org/10.1016/s0040-1951(03)00232-4)
- Lund, M. G., Austrheim, H., & Erambert, M. (2004). Earthquakes in the deep continental crust—insights from studies on exhumed high-pressure rocks. *Geophysical Journal International*, 158(2), 569–576. <https://doi.org/10.1111/j.1365-246x.2004.02368.x>
- Malvoisin, B., Austrheim, H., Hetényi, G., Reynes, J., Hermann, J., Baumgartner, L. P., & Podladchikov, Y. Y. (2020). Sustainable densification of the deep crust. *Geology*, 48(7), 673–677. <https://doi.org/10.1130/g47201.1>
- Malvoisin, B., Brantut, N., & Kaczmarek, M.-A. (2017). Control of serpentinisation rate by reaction-induced cracking. *Earth and Planetary Science Letters*, 476, 143–152. <https://doi.org/10.1016/j.epsl.2017.07.042>
- Malvoisin, B., Podladchikov, Y. Y., & Myasnikov, A. V. (2021). Achieving complete reaction while the solid volume increases: A numerical model applied to serpentinisation. *Earth and Planetary Science Letters*, 563, 116859. <https://doi.org/10.1016/j.epsl.2021.116859>
- Mancktelow, N. S., & Pennacchioni, G. (2005). The control of precursor brittle fracture and fluid–rock interaction on the development of single and paired ductile shear zones. *Journal of Structural Geology*, 27(4), 645–661. <https://doi.org/10.1016/j.jsg.2004.12.001>
- Mansard, N., Stünitz, H., Raimbourg, H., & Précigout, J. (2020). The role of deformation–reaction interactions to localize strain in polymineralic rocks: Insights from experimentally deformed plagioclase–pyroxene assemblages. *Journal of Structural Geology*, 134, 104008. <https://doi.org/10.1016/j.jsg.2020.104008>
- Marti, S., Stünitz, H., Heilbronner, R., Plümper, O., & Drury, M. (2017). Experimental investigation of the brittle–viscous transition in mafic rocks—Interplay between fracturing, reaction, and viscous deformation. *Journal of Structural Geology*, 105, 62–79. <https://doi.org/10.1016/j.jsg.2017.10.011>
- Marti, S., Stünitz, H., Heilbronner, R., Plümper, O., & Kilian, R. (2018). Syn-kinematic hydration reactions, grain size reduction, and dissolution–precipitation creep in experimentally deformed plagioclase–pyroxene mixtures. *Solid Earth*, 9(4), 985–1009. <https://doi.org/10.5194/se-9-985-2018>
- Meike, A. (1993). A critical review of investigations into transformation plasticity. *Defects and Processes in the Solid State: Geoscience Applications, The McLaren*, 5–25.
- Menegon, L., Campbell, L., Mancktelow, N., Camacho, A., Wex, S., Papa, S., et al. (2021). The earthquake cycle in the dry lower continental crust: Insights from two deeply exhumed terranes (Musgrave Ranges, Australia and Lofoten, Norway). *Philosophical transactions of the Royal Society A*, 379(2193), 20190416. <https://doi.org/10.1098/rsta.2019.0416>
- Menegon, L., Pennacchioni, G., Malaspina, N., Harris, K., & Wood, E. (2017). Earthquakes as precursors of ductile shear zones in the dry and strong lower crust. *Geochemistry, Geophysics, Geosystems*, 18(12), 4356–4374. <https://doi.org/10.1002/2017gc007189>
- Mitra, G. (1978). Ductile deformation zones and mylonites; the mechanical processes involved in the deformation of crystalline basement rocks. *American Journal of Science*, 278(8), 1057–1084. <https://doi.org/10.2475/ajs.278.8.1057>
- Moresi, L., Dufour, F., & Mühlhaus, H. (2021). Viscoelastic formulation for modeling of plate tectonics. In *Bifurcation and localisation theory in geomechanics* (pp. 337–343). CRC Press.
- Murrell, S., & Ismail, I. (1976). The effect of decomposition of hydrous minerals on the mechanical properties of rocks at high pressures and temperatures. *Tectonophysics*, 31(3–4), 207–258. [https://doi.org/10.1016/0040-1951\(76\)90120-7](https://doi.org/10.1016/0040-1951(76)90120-7)
- Nakajima, J., Uchida, N., Shiina, T., Hasegawa, A., Hacker, B. R., & Kirby, S. H. (2013). Intermediate-depth earthquakes facilitated by eclogitization-related stresses. *Geology*, 41(6), 659–662. <https://doi.org/10.1130/g33796.1>
- Newman, J., Chatzaras, V., Tikoff, B., Wijbrans, J. R., Lamb, W. M., & Drury, M. R. (2021). Strain localization at constant strain rate and changing stress conditions: Implications for plate boundary processes in the upper mantle. *Minerals*, 11(12), 1351. <https://doi.org/10.3390/min11121351>
- Newman, J., Lamb, W. M., Drury, M. R., & Vissers, R. L. (1999). Deformation processes in a peridotite shear zone: Reaction-softening by an H₂O-deficient, continuous net transfer reaction. *Tectonophysics*, 303(1–4), 193–222. [https://doi.org/10.1016/s0040-1951\(98\)00259-5](https://doi.org/10.1016/s0040-1951(98)00259-5)
- Okazaki, K., & Hirth, G. (2016). Dehydration of lawsonite could directly trigger earthquakes in subducting oceanic crust. *Nature*, 530(7588), 81–84. <https://doi.org/10.1038/nature16501>
- Olgaard, D. L., Ko, S.-C., & Wong, T.-F. (1995). Deformation and pore pressure in dehydrating gypsum under transiently drained conditions. *Tectonophysics*, 245(3–4), 237–248. [https://doi.org/10.1016/0040-1951\(94\)00237-4](https://doi.org/10.1016/0040-1951(94)00237-4)
- Oliot, E., Goncalves, P., & Marquer, D. (2010). Role of plagioclase and reaction softening in a metagranite shear zone at mid-crustal conditions (Gotthard Massif, Swiss Central Alps). *Journal of Metamorphic Geology*, 28(8), 849–871. <https://doi.org/10.1111/j.1525-1314.2010.00897.x>
- Omori, S., Komabayashi, T., & Maruyama, S. (2004). Dehydration and earthquakes in the subducting slab: Empirical link in intermediate and deep seismic zones. *Physics of the Earth and Planetary Interiors*, 146(1–2), 297–311. <https://doi.org/10.1016/j.pepi.2003.08.014>
- Pabst, W., Gregorova, E., Rambaldi, E., & Bignozzi, M. C. (2015). Effective elastic constants of plagioclase feldspar aggregates in dependence of the anorthite content—a concise review. *Ceramics–Silikáty*, 59(4), 326–330.
- Paterson, M. (1989). The interaction of water with quartz and its influence in dislocation flow—An overview. *Rheology of Solids and of the Earth*, 107–142.
- Poirier, J. (1982). On transformation plasticity. *Journal of Geophysical Research*, 87(B8), 6791–6797. <https://doi.org/10.1029/jb087ib08p06791>
- Précigout, J., Gueydan, F., Gapais, D., Garrido, C., & Essai, A. (2007). Strain localisation in the subcontinental mantle—A ductile alternative to the brittle mantle. *Tectonophysics*, 445(3–4), 318–336. <https://doi.org/10.1016/j.tecto.2007.09.002>
- Raleigh, C., & Paterson, M. (1965). Experimental deformation of serpentinite and its tectonic implications. *Journal of Geophysical Research*, 70(16), 3965–3985. <https://doi.org/10.1029/jz070i16p03965>
- Rogowitz, A., & Huet, B. (2021). Evolution of fluid pathways during eclogitization and their impact on formation and deformation of eclogite: A microstructural and petrological investigation at the type locality (Koralpe, Eastern Alps, Austria). *Tectonophysics*, 819, 229079. <https://doi.org/10.1016/j.tecto.2021.229079>
- Rogowitz, A., Schorn, S., & Huet, B. (2024). Eclogite dehydration and melt-induced embrittlement at high-pressure conditions. *Terra Nova*, 36(4), 266–274. <https://doi.org/10.1111/ter.12707>
- Rogowitz, A., Thielmann, M., Kraus, K., Grasemann, B., & Renner, J. (2023). The effect of the garnet content on deformation mechanisms and weakening of eclogite: Insights from deformation experiments and numerical simulations. *Geochemistry, Geophysics, Geosystems*, 24(3), e2022GC010743. <https://doi.org/10.1029/2022gc010743>
- Rubie, D. (1983). Reaction-enhanced ductility: The role of solid–solid univariant reactions in deformation of the crust and mantle. *Tectonophysics*, 96(3–4), 331–352. [https://doi.org/10.1016/0040-1951\(83\)90225-1](https://doi.org/10.1016/0040-1951(83)90225-1)
- Rubie, D. (1990). Reaction enhanced deformability. In *Deformation processes in minerals, ceramics and rocks* (pp. 262–292). Mineralogical Society, Unwin Hyman.
- Rubie, D. (1998). Disequilibrium during metamorphism: The role of nucleation kinetics. *Geological Society, London, Special Publications*, 138(1), 199–214. <https://doi.org/10.1144/gsl.sp.1996.138.01.12>

- Rubie, D., & Thompson, A. (1985). Kinetics of metamorphic reactions at elevated temperatures and pressures: An appraisal of available experimental data. In *Metamorphic reactions: Kinetics, textures, and deformation* (pp. 27–79). Springer.
- Rutter, E., & Brodie, K. (1988a). Experimental “syctectonic” dehydration of serpentinite under conditions of controlled pore water pressure. *Journal of Geophysical Research*, 93(B5), 4907–4932. <https://doi.org/10.1029/jb093ib05p04907>
- Rutter, E., & Brodie, K. (1988b). The role of tectonic grain size reduction in the rheological stratification of the lithosphere. *Geologische Rundschau*, 77(1), 295–307. <https://doi.org/10.1007/bf01848691>
- Rybacki, E., & Dresen, G. (2000). Dislocation and diffusion creep of synthetic anorthite aggregates. *Journal of Geophysical Research*, 105(B11), 26017–26036. <https://doi.org/10.1029/2000jb900223>
- Scambelluri, M., Pennacchioni, G., Gilio, M., Bestmann, M., Plümper, O., & Nestola, F. (2017). Fossil intermediate-depth earthquakes in subducting slabs linked to differential stress release. *Nature Geoscience*, 10(12), 960–966. <https://doi.org/10.1038/s41561-017-0010-7>
- Schmalholz, S. M., Moulas, E., Plümper, O., Myasnikov, A. V., & Podladchikov, Y. Y. (2020). 2D hydro-mechanical-chemical modeling of (de)hydration reactions in deforming heterogeneous rock: The periclase-brucite model reaction. *Geochemistry, Geophysics, Geosystems*, 21(11), e2020GC009351. <https://doi.org/10.1029/2020gc009351>
- Schmidt, C., Bruhn, D., & Wirth, R. (2003). Experimental evidence of transformation plasticity in silicates: Minimum of creep strength in quartz. *Earth and Planetary Science Letters*, 205(3–4), 273–280. [https://doi.org/10.1016/s0012-821x\(02\)01046-4](https://doi.org/10.1016/s0012-821x(02)01046-4)
- Scholz, C. H., & Choi, E. (2022). What comes first: The fault or the ductile shear zone? *Earth and Planetary Science Letters*, 577, 117273. <https://doi.org/10.1016/j.epsl.2021.117273>
- Segall, P., & Simpson, C. (1986). Nucleation of ductile shear zones on dilatant fractures. *Geology*, 14(1), 56–59. [https://doi.org/10.1130/0091-7613\(1986\)14<56:nodszo>2.0.co;2](https://doi.org/10.1130/0091-7613(1986)14<56:nodszo>2.0.co;2)
- Shi, F., Wang, Y., Wen, J., Yu, T., Zhu, L., Huang, T., & Wang, K. (2022). Metamorphism-facilitated faulting in deforming orthopyroxene: Implications for global intermediate-depth seismicity. *Proceedings of the National Academy of Sciences*, 119(11), e2112386119. <https://doi.org/10.1073/pnas.2112386119>
- Shi, F., Wang, Y., Yu, T., Zhu, L., Zhang, J., Wen, J., et al. (2018). Lower-crustal earthquakes in southern Tibet are linked to eclogitization of dry metastable granulite. *Nature Communications*, 9(1), 1–13. <https://doi.org/10.1038/s41467-018-05964-1>
- Snow, E., & Yund, R. A. (1987). The effect of ductile deformation on the kinetics and mechanisms of the aragonite-calcite transformation. *Journal of Metamorphic Geology*, 5(2), 141–153. <https://doi.org/10.1111/j.1525-1314.1987.tb00376.x>
- Steltenpohl, M. G., Kassos, G., & Andresen, A. (2006). Retrograded eclogite-facies pseudotachylytes as deep-crustal paleoseismic faults within continental basement of Lofoten, north Norway. *Geosphere*, 2(1), 61–72. <https://doi.org/10.1130/ges00035.1>
- Stünitz, H., & Gerald, J. F. (1993). Deformation of granulitoids at low metamorphic grade. II: Granular flow in albite-rich mylonites. *Tectonophysics*, 221(3–4), 299–324. [https://doi.org/10.1016/0040-1951\(93\)90164-f](https://doi.org/10.1016/0040-1951(93)90164-f)
- Stünitz, H., Neufeld, K., Heilbronner, R., Finstad, A. K., Konopásek, J., & Mackenzie, J. R. (2020). Transformation weakening: Diffusion creep in eclogites as a result of interaction of mineral reactions and deformation. *Journal of Structural Geology*, 139, 104129. <https://doi.org/10.1016/j.jsg.2020.104129>
- Stünitz, H., & Tullis, J. (2001). Weakening and strain localization produced by syn-deformational reaction of plagioclase. *International Journal of Earth Sciences*, 90(1), 136–148. <https://doi.org/10.1007/s005310000148>
- Thielmann, M. (2018). Grain size assisted thermal runaway as a nucleation mechanism for continental mantle earthquakes: Impact of complex rheologies. *Tectonophysics*, 746, 611–623. <https://doi.org/10.1016/j.tecto.2017.08.038>
- Thielmann, M., Rozel, A., Kaus, B., & Ricard, Y. (2015). Intermediate-depth earthquake generation and shear zone formation caused by grain size reduction and shear heating. *Geology*, 43(9), 791–794. <https://doi.org/10.1130/g36864.1>
- Tullis, J., Dell’Angelo, L., & Yund, R. A. (1990). Ductile shear zones from brittle precursors in feldspathic rocks: The role of dynamic recrystallization. *The Brittle-Ductile Transition in Rocks*, 56, 67–81. <https://doi.org/10.1029/gm056p0067>
- Tullis, J., & Yund, R. A. (1980). Hydrolytic weakening of experimentally deformed Westerly granite and Hale albite rock. *Journal of Structural Geology*, 2(4), 439–451. [https://doi.org/10.1016/0191-8141\(80\)90005-x](https://doi.org/10.1016/0191-8141(80)90005-x)
- Ulven, O., Storheim, H., Austrheim, H., & Malthe-Sørenssen, A. (2014). Fracture initiation during volume increasing reactions in rocks and applications for CO₂ sequestration. *Earth and Planetary Science Letters*, 389, 132–142. <https://doi.org/10.1016/j.epsl.2013.12.039>
- Wayte, G. J., Worden, R. H., Rubie, D. C., & Droop, G. T. (1989). A TEM study of disequilibrium plagioclase breakdown at high pressure: The role of infiltrating fluid. *Contributions to Mineralogy and Petrology*, 101(4), 426–437. <https://doi.org/10.1007/bf00372216>
- Wenk, H.-R., & Pannetier, J. (1990). Texture development in deformed granodiorites from the Santa Rosa mylonite zone, southern California. *Journal of Structural Geology*, 12(2), 177–184. [https://doi.org/10.1016/0191-8141\(90\)90003-h](https://doi.org/10.1016/0191-8141(90)90003-h)
- White, S. t., & Knipe, R. (1978). Transformation-and reaction-enhanced ductility in rocks. *Journal of the Geological Society*, 135(5), 513–516. <https://doi.org/10.1144/gsjgs.135.5.0513>
- Xiao, X., Wirth, R., & Dresen, G. (2002). Diffusion creep of anorthite-quartz aggregates. *Journal of Geophysical Research*, 107(B11), 2279. <https://doi.org/10.1029/2001jb000789>
- Yamato, P., Duret, T., & Angiboust, S. (2019). Brittle/ductile deformation of eclogites: Insights from numerical models. *Geochemistry, Geophysics, Geosystems*, 20(7), 3116–3133. <https://doi.org/10.1029/2019gc008249>
- Yamato, P., Duret, T., Baïssat, M., & Luisier, C. (2022). Reaction-induced volume change triggers brittle failure at eclogite facies conditions. *Earth and Planetary Science Letters*, 584, 117520. <https://doi.org/10.1016/j.epsl.2022.117520>
- Yamato, P., Tartese, R., Duret, T., & May, D. A. (2012). Numerical modelling of magma transport in dykes. *Tectonophysics*, 526, 97–109. <https://doi.org/10.1016/j.tecto.2011.05.015>
- Zertani, S., John, T., Brachmann, C., Vrijmoed, J. C., & Plümper, O. (2022). Reactive fluid flow guided by grain-scale equilibrium reactions during eclogitization of dry crustal rocks. *Contributions to Mineralogy and Petrology*, 177(6), 61. <https://doi.org/10.1007/s00410-022-01928-3>
- Zheng, X., Cordonnier, B., McBeck, J., Boller, E., Jamtveit, B., Zhu, W., & Renard, F. (2019). Mixed-mode strain localization generated by hydration reaction at crustal conditions. *Journal of Geophysical Research: Solid Earth*, 124(5), 4507–4522. <https://doi.org/10.1029/2018jb017008>